AGU PUBLICATIONS

JGR

Journal of Geophysical Research: Atmospheres

RESEARCH ARTICLE
10.1002/2016JD025039

Key Points:
- Amazon convective diurnal cycle characteristics vary with convective intensity
- Column humidity is the most important factor explaining convective behavior
- CAPE is a poor predictor of the Amazonian convective diurnal cycle

Correspondence to:
K. F. Itterly,
kyle.f.itterly@nasa.gov

Citation:
Itterly, K. F., P. C. Taylor, J. B. Dodson, and A. B. Tawfik (2016), On the sensitivity of the diurnal cycle in the Amazon to convective intensity, *J. Geophys. Res. Atmos.*, *121*, 8186–8208, doi:10.1002/2016JD025039.

Received 4 MAR 2016
Accepted 29 JUN 2016
Accepted article online 4 JUL 2016
Published online 19 JUL 2016

On the sensitivity of the diurnal cycle in the Amazon to convective intensity

Kyle F. Itterly[1], Patrick C. Taylor[2], Jason B. Dodson[2], and Ahmed B. Tawfik[3]

[1]Science Systems and Applications, Inc., Hampton, Virginia, USA, [2]Climate Science Branch, NASA Langley Research Center, Hampton, Virginia, USA, [3]Climate and Global Dynamics, National Center for Atmospheric Research, Boulder, Colorado, USA

Abstract Climate and reanalysis models contain large water and energy budget errors over tropical land related to the misrepresentation of diurnally forced moist convection. Motivated by recent work suggesting that the water and energy budget is influenced by the sensitivity of the convective diurnal cycle to atmospheric state, this study investigates the relationship between convective intensity, the convective diurnal cycle, and atmospheric state in a region of frequent convection—the Amazon. Daily, 3-hourly satellite observations of top of atmosphere (TOA) fluxes from Clouds and the Earth's Radiant Energy System Ed3a SYN1DEG and precipitation from Tropical Rainfall Measuring Mission 3B42 data sets are collocated with twice daily Integrated Global Radiosonde Archive observations from 2002 to 2012 and hourly flux tower observations. Percentiles of daily minimum outgoing longwave radiation are used to define convective intensity regimes. The results indicate a significant increase in the convective diurnal cycle amplitude with increased convective intensity. The TOA flux diurnal phase exhibits 1–3 h shifts with convective intensity, and precipitation phase is less sensitive. However, the timing of precipitation onset occurs 2–3 h earlier and the duration lasts 3–5 h longer on very convective compared to stable days. While statistically significant changes are found between morning atmospheric state and convective intensity, variations in upper and lower tropospheric humidity exhibit the strongest relationships with convective intensity and diurnal cycle characteristics. Lastly, convective available potential energy (CAPE) is found to vary with convective intensity but does not explain the variations in Amazonian convection, suggesting that a CAPE-based convective parameterization will not capture the observed behavior without incorporating the sensitivity of convection to column humidity.

1. Introduction

The diurnal cycle of deep convection in the Amazon significantly impacts the climatological water cycle and energy budget in the Tropics [*Bergman and Salby*, 1997; *Yang and Slingo*, 2001; *Zhang and Klein*, 2010; *Taylor*, 2012a]. The largest climatological diurnal amplitude of clouds and precipitation is observed over Tropical land convective regions where the climatological diurnal phase of deep convection occurs in the midafternoon [*Dai*, 2001; *Yang and Slingo*, 2001; *Nesbitt and Zipser*, 2003]. The development of afternoon deep convection is constrained by the coupling of the planetary boundary layer (PBL) to the overlying free tropospheric state [*Derbyshire et al*., 2004; *Kuang and Bretherton*, 2006; *Zhang and Klein*, 2010; *Tawfik and Dirmeyer*, 2014]. Due in part to a lack of atmospheric state observations, the sensitivity of this coupling is poorly understood in Tropical moist convective regions [*Betts*, 2000] resulting in large errors in the simulated energy budget and water cycle [*Lin et al*., 2000; *Betts and Jakob*, 2002b; *Itterly and Taylor*, 2014].

Climate and meteorological reanalysis models fail to reproduce the observed amplitude and timing of the convective diurnal cycle in the Amazon and other tropical regions where moist convection dominates [*Betts and Jakob*, 2002b]. Simulated diurnal precipitation maxima occur shortly before local noon, 2–4 h earlier than observations [*Lin et al*., 2000; *Betts and Jakob*, 2002b; *Collier and Bowman*, 2004; *Dai and Trenberth*, 2004]. This misrepresentation contributes to biases in the simulated top of atmosphere (TOA) energy budget [*Bergman and Salby*, 1997; *Taylor*, 2014a, 2014b; *Itterly and Taylor*, 2014]. The inability of climate models to correctly capture diurnally forced tropical moist convection is a major stumbling block in climate simulation [*Yang and Slingo*, 2001; *Randall et al*., 2003; *Arakawa*, 2004; *Schlemmer et al*., 2011; *Taylor*, 2012b].

Traditional diurnal cycle analysis considers the diurnal cycle as a monthly or climatological average of each hourly interval, ignoring the influence of "daily weather noise" [*Yang and Slingo*, 2001]. Recent work suggests a physically significant influence of atmospheric state on the convective diurnal cycle affecting both the mean state and variability of the energy budget and water cycle [*Strong et al*., 2005; *Pereira and Rutledge*, 2006;

Zhang and Klein, 2010; *Taylor*, 2014a, 2014b; *Dodson and Taylor*, 2016]. The recent results suggest that the climatological diurnal cycle can be represented by a combination of statistically different diurnal cycles distinguished by atmospheric state. A gap in our current knowledge is how characteristics of the convective diurnal cycle vary with atmospheric state and convective intensity.

The present study utilizes daily observations to relate diurnal characteristics of outgoing longwave radiation (OLR), longwave cloud forcing (LWCF), shortwave cloud forcing (SWCF), and precipitation to atmospheric state for five regimes of convective intensity in the wet season (December-January-February (DJF)) and the dry season (June-July-August (JJA)) in the Amazon. The objectives of this study are to (i) describe the sensitivity of the TOA flux, surface flux, and precipitation diurnal cycles to convective intensity and (ii) characterize the relationships between preconvective atmospheric state and the convective diurnal cycle for eight stations in the wet and dry seasons. Section 2 provides a brief overview of the Amazonian convective diurnal cycle. Sections 3 and 4 describe the data and methodology, respectively. Section 5 presents the results, illustrating the relationships between convective intensity, the convective diurnal cycle, and atmospheric state. A discussion is provided in section 6 and summary and conclusions in section 7.

2. Background

Extensive research and field campaigns have investigated the physical processes driving Amazonian convection with a focus on the diurnal cycle of precipitation, clouds and radiation [*Lin et al*., 2000; *Betts*, 2000; *Betts and Jakob*, 2002a, 2002b; *Betts et al*., 2002; *Machado et al*., 2002; *Strong et al*., 2005; *Machado et al*., 2014; *Tanaka et al*., 2014; *Taylor*, 2014a, 2014b; *Dodson and Taylor*, 2016].

Planetary boundary layer (PBL) characteristics, related to surface processes, provide important information regarding the priming of the atmosphere for convective initiation [*Betts et al*., 2009; *Santanello et al*., 2009; *Zhang and Klein*, 2010; *Tawfik and Dirmeyer*, 2014]. The PBL conditions that precede moist convection in the Amazon resemble those found over the tropical oceans due to high surface humidity sustained by thick vegetation and soil moisture storage [*Betts et al*., 2009; *Dirmeyer*, 2011]. The Amazonian boundary layer, as a result, exhibits a low-lifted condensation level (LCL) similar to tropical oceanic regions [*Betts et al*., 2009], enabling frequent afternoon convection as the land surface is heated.

The diurnal evolution of the PBL is a function of the interplay between surface fluxes and the vertical profile of the overlaying atmosphere and advection [*Holtslag and Moeng*, 1991; *Betts*, 2000; *Ek and Holtslag*, 2004; *Betts et al*., 2009; *Trier et al*., 2008; *Santanello et al*., 2009; *van Heerwaarden et al*., 2010; *Tawfik and Dirmeyer*, 2014]. At sunrise, the convective boundary layer begins accumulating energy from solar insolation, which drives turbulent circulations producing a well-mixed boundary layer. Once the mixed layer depth reaches the LCL, buoyant parcels condense forming low-level cumulus clouds. With sufficient instability and solar heating, cumuli deepen and evolve into cumuli congesti.

Convective initiation tends to occur when the layer between the LCL and the level of free convection (LFC) becomes sufficiently moistened by the presence of shallow cumulus to reduce the effects of dry air entrainment [*Chaboureau et al*., 2004]. Upon reaching the LFC, vertical motion of air parcels is uninhibited until reaching the equilibrium level (EL) where convective detrainment occurs, promoting the formation of convective anvil clouds. After maximum rainfall, the atmospheric profile has reached a near-saturated state; surface and water vapor fluxes decrease in the PBL, and deep convection dissipates when convective inhibition (CIN) exceeds the vertical kinetic energy [*Chaboureau et al*., 2004; *Machado et al*., 2014].

Previous work quantifying the amplitude and timing of the convective diurnal cycle describes the convective diurnal cycle in the Amazon by the following general behavior. *Tanaka et al*. [2014] found that the hours of the day with the highest climatological precipitation frequency occur between 12:00 and 17:00 local solar time (LST) for stations in central Brazil. *Taylor* [2012a] indicated that the maximum LWCF in the Amazon occurs between 18:00 and 20:00 LST just after the maximum precipitation rate.

Machado et al. [2002] describe the diurnal cycle of cloud and precipitation processes in the wet season using a combination of satellite, surface, and radiosonde observations during the Tropical Rainfall Measuring Mission Large-Scale Biosphere-Atmosphere (TRMM-LBA) field experiment in the Rondônia state of southwestern Brazil. The most intense climatological convection is observed in Rondônia during the wet season, as moisture from the north and east converges along the Andes and is transported southward toward the

midlatitudes by a low-level jet (LLJ) [*Machado et al*., 2002]. The diurnal minimum deep convective cloud fraction (0%) and high cloud fraction (3%) are observed just before 12:00 LST, followed by a rapid increase in deep convective clouds, high clouds, and precipitation. Deep convective and high clouds peak around 17:00 LST (6% and 29%, respectively) and gradually dissipate after 18:00 LST. Vigorous convection dissipates rapidly, while remnant anvils and mesoscale convective systems linger for several more hours. Total cloud cover reaches its diurnal minimum at 12:30 LST (56%) as convective clouds experience their largest diurnal rate of increase. Total cloud cover builds through the evening, reaching diurnal maximum (94%) overnight at 03:30 LST. The diurnal maximum rain fraction occurs between 13:30 and 15:30 LST with a smaller, secondary overnight peak of less intense rainfall rates at 03:30 LST coinciding with the maximum total cloud fraction.

Recent studies, however, highlight deviations from the general convective diurnal cycle in the Amazon. *Strong et al*. [2005] identify distinctive diurnal patterns in low-level cloud and subcloud layer properties by wind regime using data from TRMM-LBA. A westerly flow regime is associated with a cooler, moister subcloud layer with reduced buoyancy effects and a predominately stratiform cloud field. An easterly flow regime is associated with higher probabilities of convection, increased buoyancy flux, increased latent heat flux, and a predominately cumuliform cloud field. These distinct large-scale flow regimes observed during TRMM-LBA have been the focus of similar studies [*Betts and Jakob*, 2002a; *Rickenbach*, 2004; *Pereira and Rutledge*, 2006]. Additionally, *Taylor* [2014a, 2014b] indicates that the variability in the Amazonian convective diurnal cycle in response to variations in atmospheric state contributes as much as 20% to the interannual TOA flux variability.

The Amazon region contains large variations in surface type influencing the precipitation characteristics. Large regional differences have been observed in the total precipitation for forest and city stations, with forest stations receiving about 20% more rainfall climatologically [*Tanaka et al*., 2014]. Seasonal differences in rainfall are also large for all stations. Rainfall frequency is approximately three times larger in the wet season than the dry season, which is caused by more frequent rainfall events as opposed to higher rainfall intensities [*Tanaka et al*., 2014].

Diurnally forced coastal squall lines from a land-sea breeze circulation are an important climatological feature in northeastern Brazil. These features propagate inland at varying distances depending on thermodynamic and dynamic background states [*Cohen et al*., 1995] and are important mechanisms for transporting oceanic moisture inland. The organization of these coastal systems makes them more predictable than moist convection in the Amazonian interior.

3. Data

3.1. CERES SYN Radiative Fluxes

The Clouds and the Earth's Radiant Energy System (CERES) Ed3a SYN1DEG Terra+Aqua data set contains TOA and surface radiative fluxes and cloud fraction retrievals extending from July 2002 to the present (with a 6 month processing lag) at $1° \times 1°$ spatial resolution and 3-hourly temporal resolution [*Loeb et al*., 2009; *Doelling et al*., 2013]. The cloud radiative effect is given by the LWCF and SWCF, where $\mathrm{LWCF} = \mathrm{OLR}_{\mathrm{CLR}} - \mathrm{OLR}$ and $\mathrm{SWCF} = \mathrm{RSW}_{\mathrm{CLR}} - \mathrm{RSW}$ [*Taylor*, 2014a]. RSW refers to the reflected shortwave radiation at TOA and the subscript CLR refers to the TOA flux in the absence of clouds, called the clear-sky flux. For simplicity, we use the absolute value of SWCF in this study.

The CERES SYN1DEG product fuses CERES Terra and Aqua Sun-synchronous fluxes with geostationary (GEO)-observed radiances to achieve 3-hourly resolution [*Doelling et al*., 2013]. The merging technique involves several steps: (1) a calibration of each GEO instrument with MODIS imager data, (2) a narrow band to broadband radiance conversion, (3) an integration of GEO broadband radiance to irradiance, and (4) a normalization of GEO-derived flux to observed CERES flux. Uncertainties in the CERES SYN data are independent of local time [*Doelling et al*., 2013]. The largest flux errors occur in desert regions, ~10% overestimate in the morning TOA fluxes. This feature is consistent from month to month due to the consistency of GEO satellite view angles. *Doelling et al*. [2013] provide a detailed description of these data.

3.2. TRMM 3B42 Precipitation Rate

TRMM-adjusted merged-infrared (IR) precipitation 3B42 data set provides precipitation data. The native spatial resolution is 0.25° by 0.25° with 3-hourly temporal resolution and coverage extending from 50°S to 50°N. The 3B42 precipitation algorithm consists of two steps. The first step uses TRMM VIRS infrared and TMI orbit

Table 1. Descriptive Statistics of the Radiosonde Stations Used to Calculate Convective Parameters Along With Collocated TRMM and CERES Data[a]

Station	Latitude (°S)	Longitude (°W)	Elevation (m)	DJF (JJA) Mean Precipitation (mm d^{-1})	DJF (JJA) Mean OLR (W m^{-2})	DJF (JJA) 12:00 UTC No. of Observation	DJF (JJA) TRMM RMS
Belem	−1.4	−48.5	16.0	9.5 (5.5)	216.3 (265.9)	700 (817)	2.7 (2.1)
Manaus	−3.2	−60.0	84.0	8.1 (2.8)	205.8 (255.5)	784 (842)	1.2 (0.7)
Alta	−8.7	−63.9	288.0	11.8 (0.4)	201.4 (283.4)	560 (537)	2.2 (.4)
Porto	−9.9	−56.1	102.0	10.1 (0.9)	202.6 (275.0)	627 (717)	1.9 (0.5)
Vilhena	−12.7	−60.1	612.0	10.3 (0.5)	200.6 (280.4)	562 (779)	2.3 (0.4)
Carolina	−7.3	−47.5	185.0	8.3 (0.2)	211.8 (288.7)	458 (357)	1.8 (0.3)
Leticia	−4.6	−69.5	84.0	11.3 (4.9)	202.2 (248.4)	357 (298)	2.1 (1.3)
Cayenne	4.8	−52.4	9.0	7.7 (6.1)	240.3 (251.6)	962 (982)	1.4 (1.0)

[a]JJA, June-July-August.

data (TRMM products 1B01 and 2A12) to produce monthly IR calibration parameters. The second step uses the monthly calibration parameters to adjust the merged-IR precipitation data retrieved from GMS, GOES-E, GOES-W, Meteosat-7, Meteosat-5, and NOAA 12 [*Kummerow et al.*, 1998].

The root-mean-square (RMS) differences between TRMM 3B42 and the rain gauge sites during wet and dry seasons are listed in Table 1. Rainfall amounts and the RMS differences are larger in the wet season with RMS differences reaching 2.7 mm d^{-1}. *Smith et al.* [2006] estimate monthly indirect biases of about 0.5–1 mm d^{-1}, with standard errors typically about 20% of the mean precipitation; however, daily estimates of satellite-derived precipitation biases are not available. TRMM 3B42 has been shown to significantly underestimate warm-cloud stratiform precipitation in the Amazon [*Machado et al.*, 2014].

3.3. IGRA Radiosonde Observations

Atmospheric radiosonde observations of temperature (T), dewpoint (T_d), wind speed, and wind direction are obtained from the Integrated Global Radiosonde Archive (IGRA). IGRA is the largest global sounding data set [*Durre et al.*, 2006, 2008]. Data are collected at 00:00 UTC and 12:00 UTC, with special observation times at 06:00 UTC and 18:00 UTC for certain stations.

The geographical bounds of the Amazon region (5°N–20°S, 45–70°W) and the locations of the upper air stations used in the present analysis are displayed in Figure 1. In the wet season, Alta Floresta and Leticia are the climatologically wettest stations, and Cayenne is the driest. In the dry season, northern and coastal stations are the climatologically wettest (Cayenne, Belem, and Leticia) and southern stations are the driest (Table 1).

Radiosonde observations at 00:00 UTC (~20:00 LST) and 12:00 UTC (~08:00 LST) are available for eight stations in the domain; only morning observations are available for Leticia, CO, and Carolina, BR. The number of valid seasonal profiles per station ranges from 400 to 800.

The IGRA data set is subject to quality check procedures. Temperature values fail the Tier 1 climatological check if their standardized z score exceeds a value of 6.0 relative to the climatology [*Durre et al.*, 2008]. The radiosonde profiles are subject to additional quality checks in the present study described below.

3.4. Flux Tower Field Campaign Data

Surface turbulent heat fluxes and near-surface atmospheric state variables are obtained from a flux tower in Manaus, Brazil, through the Large-Scale Biosphere-Atmosphere Data Model Intercomparison Project (LBA-DMIP) [*De Gonçalves et al.*, 2013; *Saleska et al.*, 2013]. The flux tower is located at a tropical rainforest site approximately 60 km north of the city and radiosonde station of Manaus. A nearly continuous 1-hourly data set is available from June 1999 to September 2006. Selected fluxes and state variables include the following: sensible heat flux (SHF), latent heat flux (LHF), ground heat flux (GHF), net radiation (Rn), relative humidity (RH), precipitation rate, wind speed, and wind direction.

4. Methodology

4.1. Convective Intensity Classification

Convective intensity can be defined in many ways. Two independent definitions of convective intensity are considered. First, convective intensity is defined using daily minimum OLR or 11 μm brightness temperatures where lower values indicate more intense convection because higher cloud tops have colder temperatures

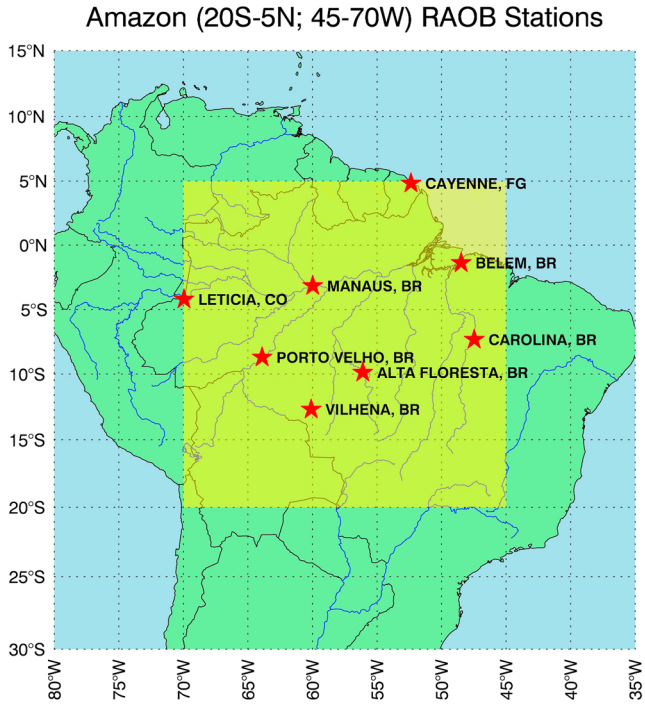

Figure 1. Spatial domain of the Amazon rainforest (yellow shading). Current operational radiosonde stations are marked with red stars. Major rivers are shown in blue.

[e.g., *Gray and Jacobson*, 1977; *Janowiak et al*., 1994]. Second, convective intensity is defined using the daily maximum precipitation rate. *Machado et al*. [2002] utilized a related definition of convective intensity using instantaneous reflectivity thresholds from ground radar data. Both definitions of convective intensity are considered to characterize the sensitivity and robustness of the results.

Daily minimum OLR and daily maximum precipitation rate exhibit different probability density functions (PDFs) and seasonality. The PDF of daily minimum OLR (Figure 2a) in the wet season is right skewed showing a longer tail for large OLR and a peak frequency at 140 W m^{-2}. For the dry season, the PDF of daily minimum OLR shows a left-skewed distribution with the peak frequency at 270 W m^{-2}. The difference in the PDF shape between the wet and dry seasons is related to differences in the frequency and intensity of convection. PDFs of daily maximum precipitation rate, unlike the minimum OLR distribution, exhibit right-skewed distributions in both seasons (Figure 2b). The primary seasonal difference is that lower precipitation rates occur more frequently in the dry season.

OLR and precipitation rate are significantly correlated. *Liebmann et al*. [1998] reported a Pearson linear correlation coefficient (r) of 0.6 between OLR and precipitation in the Amazon on 10–30 days time scales and 5° spatial scales. The correlation coefficient between daily minimum OLR and daily maximum precipitation rate at native spatial resolution is −0.46 in the wet season and −0.6 in dry season. Therefore, the two metrics of convective intensity are related to each other while exhibiting the ability to vary with respect to each other.

Convective intensity regimes are defined using percentiles of the CERES minimum OLR PDF at each grid point. The regimes are defined as very convective (<20%, VC), moderately convective (20–40%, MC), lowly convective (40–60%, LC), neutral (60–80%, N), and stable (>80%, S). Percentile definitions are used to equally distribute samples within each regime regardless of station or season. The separation of convective intensity regimes by daily minimum OLR is selected over daily maximum precipitation rates because intense nonconvective stratiform rain events in the Amazon influence the maximum precipitation PDF [*Machado et al*., 2014]. The results are found to be insensitive to the choice of convective intensity definition.

4.2. Convective Parameter Calculations

Thermodynamic and dynamic convective parameters are derived from IGRA radiosonde measurements of T, T_d, wind speed, and wind direction. Convective parameters (summarized in Table 2) include upper tropospheric

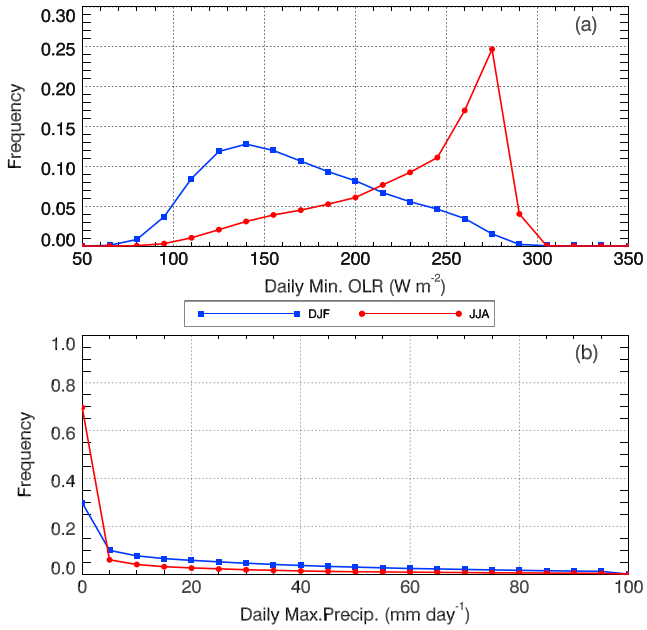

Figure 2. Probability density functions (PDFs) for the Amazon region from 2002 to 2012 for the wet season (blue) and dry season (red) for (a) CERES daily minimum OLR and (b) TRMM daily maximum precipitation rate.

humidity (UTH), lower tropospheric humidity (LTH), precipitable water (PW), convective available potential energy (CAPE), CIN, LCL, LFC, EL, lower tropospheric stability (LTS), 1000–850 hPa wind speed (WS), 1000–850 hPa average wind direction (WD), buoyant condensation level (BCL), and buoyant mixing temperature deficit (TDEF).

The BCL is defined as the height at which saturation would occur through buoyant mixing alone due to sensible heating from the surface [*Tawfik and Dirmeyer*, 2014]. The BCL can be viewed as the height that the PBL must reach for saturation to occur without the addition or removal of moisture. The buoyant mixing temperature (T_{bm}) is defined by lowering a parcel dry adiabatically from the BCL to the surface. TDEF is defined as the difference between T_{bm} and T_{2m} and quantifies the heat deficit required for triggering convection—analogous to CIN. Moist convection is initiated when TDEF = 0. This framework is independent of parcel starting height selection [*Tawfik and Dirmeyer*, 2014; *Tawfik et al.*, 2015].

CAPE and CIN are calculated as the average of all parcel heights ranging from the most unstable parcel (level with the largest equivalent potential temperature) in the lowest 500 m to the top of the mixed layer at ~1000 m above ground level (agl). This procedure minimizes bias of selecting a single parcel starting height.

Table 2. Description of Convective Parameters

Long Name	Short Name	Level 1	Level 2	Formula/Notes
Lifted condensation level	LCL	Average of lowest 500 m	NA	Equation (1)
Level of free convection	LFC	Most unstable parcel in lowest 1000 m	Level of positive buoyancy	Interpolated from level below and above
Equilibrium level	EL	LFC	Level of negative buoyancy	Interpolated from level below and above
Lower tropospheric humidity	LTH	1000 hPa	850 hPa	Pressure-weighted average RH
Upper tropospheric humidity	UTH	500 hPa	300 hPa	Log-weighted average RH
Lower tropospheric stability	LTS	900 hPa	500 hPa	Difference in equivalent potential temperature
Convectively available potential energy	CAPE	Most unstable parcel in lowest 500 m	1000 m	Average CAPE of all parcels between level 1 and level 2
Wind speed	WS	1000 hPa	850 hPa	Average wind
Wind direction	WD	1000 hPa	850 hPa	Circular average wind direction
Lapse rate	LR	900 hPa	500 hPa	$-dT/dz$
Buoyant condensation level	BCL	Surface	Height at which saturation would occur	Due to buoyant mixing alone

Folkins et al. [2014] suggest that a mass-weighted CAPE computed by selecting parcel starting heights throughout the PBL responds more slowly to diurnal warming and yields a better diurnal cycle simulation.

UTH is defined as the log-weighted average relative humidity (RH) between 500 and 300 hPa, following the weighting function explained in *Allan et al*. [1999]. LTH is defined as the pressure-weighted average RH between 1000 and 850 hPa. LTS is defined here as the equivalent potential temperature difference between 900 and 500 hPa, and LR is the temperature difference divided by the height multiplied by −1. The temperature and pressure of the LCL (T_{LCL} and P_{LCL}, respectively) are calculated using the average conditions of the lowest 500 m, and then converted into a height, using the following equations that are accurate to within a tenth of a degree [*Bolton*, 1980]:

$$T_{LCL} = \frac{1}{\frac{1}{(T_{d,500}-56)} + \frac{\ln \frac{T_{500}}{T_{d,500}}}{800}} + 56 \tag{1}$$

$$P_{LCL} = P_{500}\left(\frac{T_{LCL}}{T_{500}}\right)^{\frac{1}{k}} \tag{2}$$

where k is Poisson's constant and T_{500}, $T_{d,500}$, and P_{500} denote the average temperature, dewpoint, and pressure in the lowest 500 m agl, respectively. The units for temperature and dewpoint are in K and pressure is in hPa.

The LFC is calculated by interpolating between the level where the parcel temperature exceeds the environmental temperature and the level below, starting from the level of maximum equivalent potential temperature between 0 and 500 m agl. Similarly, the EL is approximated by interpolating between the two levels where the parcel returns to negative buoyancy in the upper troposphere and the level below.

In certain cases, radiosonde profiles lack sufficient vertical resolution to calculate convective parameters (e.g., EL and CAPE) but still pass the quality checks necessary for the near-surface parameters. The undetermined convective parameters are left undefined in this scenario. For convective parameters defined by specific heights or pressure levels (i.e., UTH, LTH, LTS, LR, WS, and WD), a range of 50 hPa is permitted in pressure for the start and end points if there is no measurement available at the desired level. The effect of allowing small ranges of values is outweighed by the statistical benefit of including more valid profiles.

A circular averaging technique is applied for directional statistics such as wind direction [*Berens*, 2009]. Considering two examples of wind directions of 359° and 1°, a simple linear average results in a value of 180° instead of 360°. Each wind direction is converted into radians (α), and cosine and sine components are summed over all angles and averaged. The arctangent of these average component angles is computed and converted back into the original units to compute the average. The standard deviation of circular statistics (σ_o) is expressed as:

$$\sigma_o = \sqrt{-2 \ln R} \tag{3}$$

where R is the resultant vector length as defined in *Berens* [2009].

For a radiosonde profile to be included in the analysis at least eight Tier 1 quality-checked levels must be present in the profile. The profile must also extend above 500 hPa and below 900 hPa to perform the necessary calculations of convective parameters.

4.3. Diurnal Cycle Composite Calculations

In this analysis, each day and 1° × 1° grid box or station is considered a realization of the convective diurnal cycle. This opposes the traditional view of the diurnal cycle where many days at a given location or region are averaged together to reduce weather noise [e.g., *Yang and Slingo*, 2001]. Using a long time average to define an average diurnal cycle does not require a specifically defined start and end time. Considering each day as a realization of the "convective diurnal cycle process" requires a specific definition. A diurnal cycle is defined to begin at sunrise and end at the next sunrise—6:00 LST to 5:59 LST—to center the analysis on the physical driver of the diurnal cycle—heating by solar insolation.

A composite diurnal cycle is calculated by averaging every 3-hourly interval for each bin of convective intensity. Error bars are displayed at each observation time, computed as the standard error displayed:

$$\text{S.E.} = \sigma(X)/\sqrt{N} \tag{4}$$

where X is all daily values of a convective parameter and N is the total number of occurrences.

The first Fourier harmonic does not adequately characterize the diurnal cycle at such high resolutions; therefore, alternate diurnal statistics are devised following *Zhang and Klein* [2010]. The diurnal phase is defined as the local time of the maximum 3-hourly interval, and the diurnal amplitude is defined as half the difference between the daily maximum and minimum values.

To explore the physical mechanisms modulating convective initiation and precipitation statistics, the onset time is defined as the 3-hourly interval where precipitation rate exceeds 10 mm d^{-1}. The duration of precipitation events is defined as the number of 3 h intervals where the precipitation rate exceeds 10 mm d^{-1}.

Composites of diurnal cycle statistics are computed in two ways. First, regionally averaged composites are computed for each diurnal statistic (i.e., amplitude, phase, and precipitation onset) in each regime and every grid point. This approach gives equal weighting to all grid points and highlights the diurnal shape of the largest climatological features. The second method focuses on the spatial variations in the sensitivities of diurnal cycle statistics. The process is very similar to the regional average composites described above, except that diurnal cycle statistics at each grid point are composited independently and displayed on a regional map.

4.4. Circular and Linear Correlation

Relationships between diurnal cycle characteristics and the 08:00 LST convective parameters from IGRA are investigated. The present study focuses on 08:00 LST convective parameters to assess how the initial atmospheric state influences the diurnal cycle evolution.

For each station and season, 08:00 LST convective parameters from radiosonde are separated into "convective" and "neutral" regimes. The VC, MC, and LC regimes are combined into a single convective regime and the N and S regimes into a neutral regime. A Pearson linear correlation coefficient is calculated for each of the combined regimes for all stations between morning convective parameters and the diurnal cycle characteristics. Correlations that are statistically significant at the 90% confidence level are shown.

An alternate correlation methodology is applied when correlating a directional atmospheric state variable such as wind direction (α) with a linear diurnal statistic (x) [*Berens*, 2009]. This method correlates cos(α) and sin(α) individually, defining correlation coefficients $r_{sx} = c(\sin(\alpha), x)$, $r_{cx} = c(\cos(\alpha), x)$, and $r_{cs} = c(\sin(\alpha), \cos(\alpha))$, where $c(x, y)$ is the Pearson correlation coefficient. The equation for circular-linear correlation (r) is defined below as

$$r = \sqrt{\frac{r_{cx}^2 + r_{sx}^2 - 2 r_{cx} r_{sx} r_{cs}}{1 - r_{cs}^2}} \tag{5}$$

5. Results

The following section is outlined as follows. First, the composite diurnal cycles of OLR, LWCF, SWCF, precipitation, surface fluxes, and surface meteorology are analyzed by convective intensity regime to identify composite relationships with the diurnal cycle. Second, composites of the atmospheric parameters that influence the diurnal cycle are discussed for each regime of convective intensity. Third, correlations between morning convective parameters and diurnal cycle characteristics are analyzed by regime, station, and season.

5.1. Relationship Between Diurnal Cycle and Convective Intensity

5.1.1. Amazon Domain Composite

Several features of the Amazon TOA flux and precipitation diurnal cycle are found to vary significantly with convective intensity. Figure 3 shows composite diurnal cycle curves of OLR, LWCF, SWCF, and precipitation within each convective intensity regime for wet and dry seasons. The composite diurnal mean total cloud cover (TCC), high cloud cover (HCC), and low cloud cover (LCC) observed by CERES by convective intensity regime and season are listed in Table 3 to provide context for the differences in TOA fluxes and precipitation across the convective intensity regimes and seasons. For all regimes, the composite TCC in the wet season (76%) is nearly twice that of the dry season (41%) (Table 3). The composite HCC is 57% on VC days in the wet season compared to 27% on VC days in the dry season, and seasonal differences in composite HCC are even more significant for less convective regimes (Table 3). Due to the limitations of observing low clouds underneath higher clouds from satellite, the composite LCC is higher in the dry season than the wet season for all convective regimes, equal for both seasons in the N regime and larger in the wet season for the S regime (Table 3).

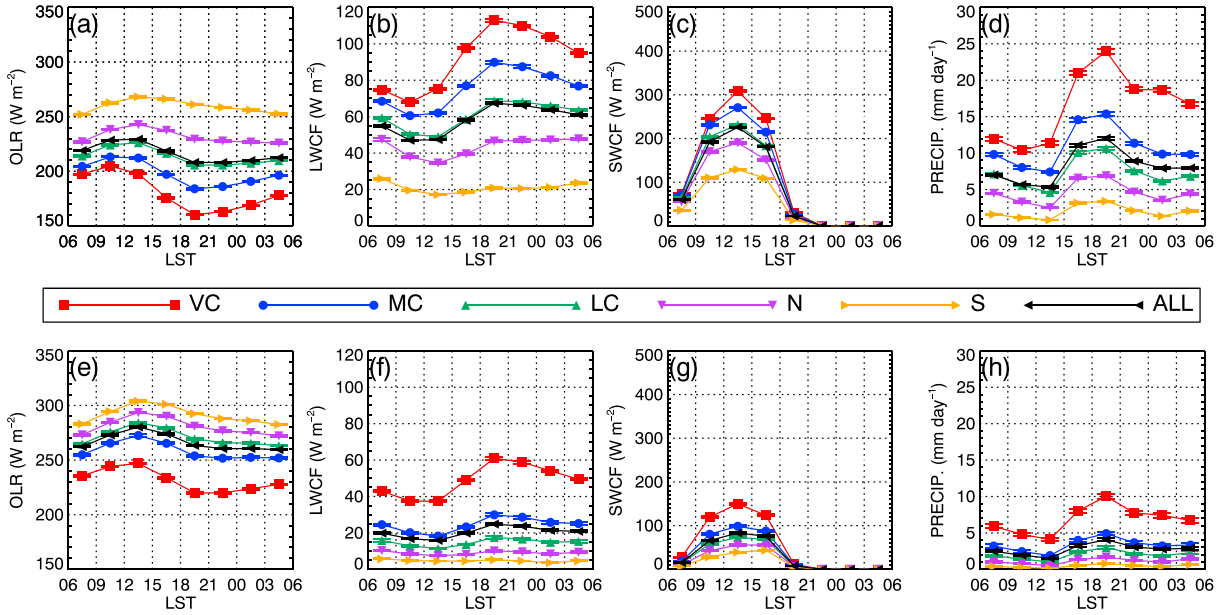

Figure 3. OLR, LWCF, SWCF, and precipitation composite diurnal cycles by convective intensity regime for the (a–d) wet season and (e–h) dry season: very convective (VC), moderately convective (MC), lowly convective (LC), neutral (N), and stable (S) and all regimes. Errors bars represent the standard error for each 3-hourly interval.

The signature of diurnally forced afternoon convection is characterized by a rapid increase (decrease) of LWCF and precipitation (OLR) shortly after noon (Figure 3). Maximum differences between diurnal composites in the wet season reach ~100 W m^{-2} for OLR and LWCF, 20 mm d^{-1} for precipitation at 18:00 LST when afternoon deep convection reaches its peak, and ~200 W m^{-2} for SWCF near noon when solar insolation reaches its peak. Precipitation and LWCF reach diurnal minimum values at 10:30 LST on VC days (red line) and at 13:30 LST for the less convective regimes (Figures 3b and 3d). Absolute differences between the VC and S regimes are smaller in the dry season, especially for precipitation (Figures 3e–33h); however, the shape of the composite diurnal cycle is similar in both seasons for all variables.

Significant variations in composite diurnal cycle statistics are shown in Figure 4 for the wet season (a and b) and dry season (c and d). The composite diurnal amplitude of OLR, LWCF, SWCF, and precipitation increases with convective intensity for both seasons (Figures 4a and 4c); a portion of this behavior is due to the increase in convective intensity itself. On VC days in the wet season, the diurnal amplitude of OLR and LWCF is ~56 W m^{-2} compared to ~42 W m^{-2} in the dry season. On S days in the wet season, the diurnal amplitude of LWCF is 18 W m^{-2} twice that of the dry season. SWCF diurnal amplitudes in the wet season range from ~170 W m^{-2} on VC days to ~80 W m^{-2} on S days and approximately half for both regimes in the dry season. Precipitation diurnal amplitudes are higher for all regimes in the wet season than the dry season (Figures 4a and 4c), especially on S days when days with near-zero precipitation are more frequent in the dry season (Figure 2b).

On VC days in the wet season, the composite OLR phase occurs at ~14:30 LST compared to ~16:00 LST on N and S days (Figure 4b). In the dry season, the OLR phase displays an opposite sensitivity to convective

Table 3. Regional Composite Diurnal Mean Total and High and Low Cloud Cover (%) by Regime of Convective Intensity for the Wet Season and Dry Season in the Amazon

	VC	MC	LC	N	S	ALL
			DJF			
TCC	90	87	81	72	51	76
HCC	57	46	36	24	12	35
LCC	13	14	15	18	21	17
			JJA			
TCC	68	50	37	30	21	41
HCC	27	12	7	4	2	11
LCC	20	24	20	18	16	20

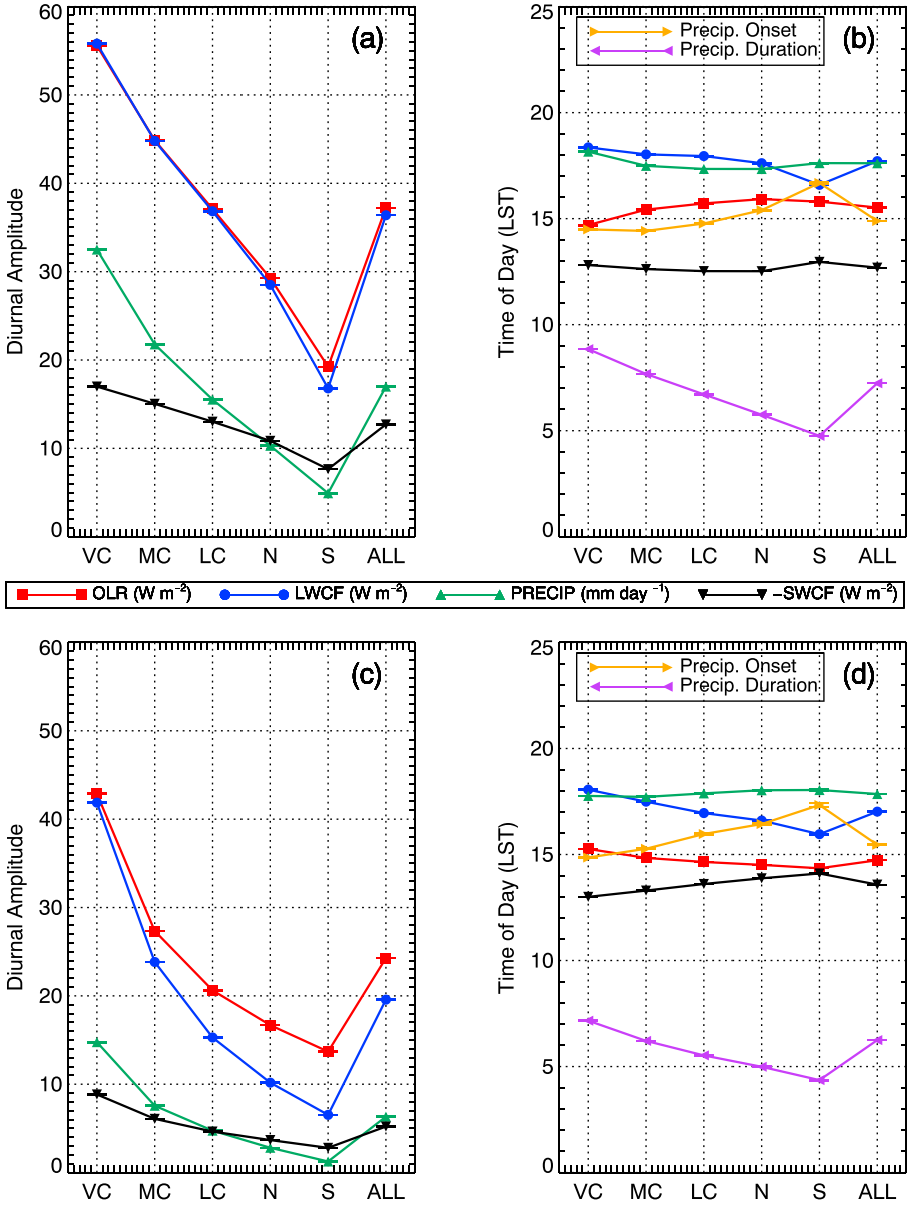

Figure 4. Regionally averaged composite OLR, LWCF, and SWCF and precipitation diurnal cycle amplitude and timing statistics are shown for the (a, b) wet season and (c, d) dry season for each convective intensity regime: very convective (VC), moderately convective (MC), lowly convective (LC), neutral (N), and stable (S) and ALL regimes. Errors bars represent the standard error for each 3-hourly interval. SWCF amplitude is divided by 10.

intensity, maximizing an hour later on convective days at ~15:30 LST compared to ~14:30 LST on stable days (Figure 4d). This behavior is primarily due to a region in Southeastern Brazil influencing the domain average results where OLR maximizes between 13:00 and 14:00 LST on S days, and little precipitation or convection is observed in the dry season (not shown). Defining the diurnal cycle between 06:00 and 05:59 LST reduces the apparent sensitivity of the OLR phase to convective intensity as OLR often maximizes in the midmorning. Using only daytime hours, the composite OLR phase occurs at ~11:00 LST on VC days and ~3 h later on S days (not shown).

Composite LWCF phase is more sensitive to convective intensity than OLR for both seasons, occurring at ~18:30 LST on VC days, ~16:30 LST on S days in the wet season (Figure 4b), and at ~18:00 LST compared to ~16:00 LST in the dry season (Figure 4d). On nonconvective days, LWCF diurnal amplitudes are small and the phase is likely determined by evolution of low clouds. Composite SWCF phase ranges between

12:30 and 13:00 LST for all regimes in the wet season and ranges between ~13:00 LST on VC days and ~14:00 LST on S days in the dry season.

Composite precipitation phase is less sensitive to convective intensity, occurring between 17:00 and 18:00 LST for all regimes and seasons (Figures 4b and 4d). The composite precipitation phase occurs ~1 h later on VC days compared to MC and LC days in the wet season (Figure 4b). This is a result of competing factors between earlier precipitation onset times and longer duration precipitation events on VC days. However, the duration and onset time of precipitation significantly varies with convective intensity.

In the wet season, the duration of convective precipitation lasts ~9 h on VC days compared to $<$5 h on S days (Figure 4b) and in the dry season for $>$7 h on VC days and ~4.5 h on S days (Figure 4d). The onset time of convective precipitation occurs ~14:30 LST on VC days in both seasons and between 17:00 and 18:00 LST on S days (Figures 4b and 4d).

5.1.2. Spatial Variation

Significant spatial variation of the Amazon convective diurnal cycle has been described in previous work [e.g., *Machado et al*., 2002]. Figure 5 illustrates the spatial composites of the convective diurnal cycle characteristics during the wet season for OLR phase (a–c), precipitation onset time (d–f), and SWCF phase (g–i) for the VC regime, S regime, and all regimes. Consideration of the spatial variations in diurnal cycle characteristics is critical for understanding the representativeness of the spatially averaged results.

Spatial variability of composite OLR phase reveals differences of 4 h across the Amazon on VC days, evident in northwest-southeast striped features (Figure 5a). The afternoon OLR phase values to the east of Manaus are related to a propagating squall line parallel to the coast on the previous day [*Cohen et al*., 1995]. A similar gradient in OLR phase, but related to topography, is evident in the southwest corner of the region for the VC regime resulting from the propagation of early afternoon convection initiated in southwestern Brazil. The spatial variations of OLR phase are less pronounced in the S regime (Figure 5b) and occur between 14:00 and 17:00 LST, consistent with the peak of surface warming under clear-sky conditions.

Composites of precipitation onset time also show significant spatial variations. On VC days, precipitation onset occurs around 12:00 LST for maritime areas, to the north of Manaus and in central Bolivia; elsewhere, precipitation begins 1–6 h later between 13:00 and 18:00 (Figure 5d). Precipitation initiates 2–4 h earlier on VC and ALL days compared to S days for most regions (Figures 5d–5f).

Spatial variability of composite SWCF phase provides a more detailed view of the progression of daytime cloud features across the region. On VC days, the composite SWCF phase occurs before noon several hundreds of kilometers inland from the coast of Northeastern Brazil (Figure 5g), as convection initiated along the coast on the previous day propagates inland. Elsewhere, composite SWCF phase occurs between 12:00 and 14:00 LST, when convective clouds experience their largest rate of increase shortly after maximum solar insolation (Figure 5g). For the S regime, spatial variability is larger across the region, with minimum values between 11:00 and 12:00 LST near the coast and in Rondônia. Later, SWCF phases between 13:30 and 15:30 LST occur in less convective areas in the northwest, southeast, and in western Bolivia (Figure 5h).

5.1.3. Diurnal Composites of Surface Terms at Manaus Flux Tower

Hourly diurnal cycle composites of surface turbulent heat fluxes and meteorological variables collected at a flux tower in Manaus, Brazil, during the LBA field campaign reveal robust sensitivities to convective intensity and season (Figure 6). The number of days in each regime is ~56 in the wet season and ~76 in the dry season; however, GHF and RH are only available for half or less of these. For both seasons, convective days are associated with decreased surface flux amplitudes and slightly earlier surface flux phases due to the presence of convective clouds (Table 3), which can act to reduce surface fluxes before maximum solar insolation (Figures 6a and 6b). Surface LHF decreases more between VC and S days than the SHF for both seasons. Rn becomes negative at 18:00 LST for both seasons but becomes more negative in the dry season due to fewer lingering overnight clouds and lower RH allowing for increased radiative cooling (Figures 6a and 6b).

Composite wind speeds are higher on S days compared to VC days for all hours of the day in both seasons (Figures 6c and 6d). Composite wind direction shows little sensitivity to convective intensity in the wet season until ~16:00–24:00 LST, when VC days favor an easterly wind and S days favor a southeasterly wind direction. In the dry season, VC days favor southwesterly winds in the morning and easterly winds in the late afternoon, whereas S days favor southerly winds in the morning and southeasterly winds in the afternoon. Composite

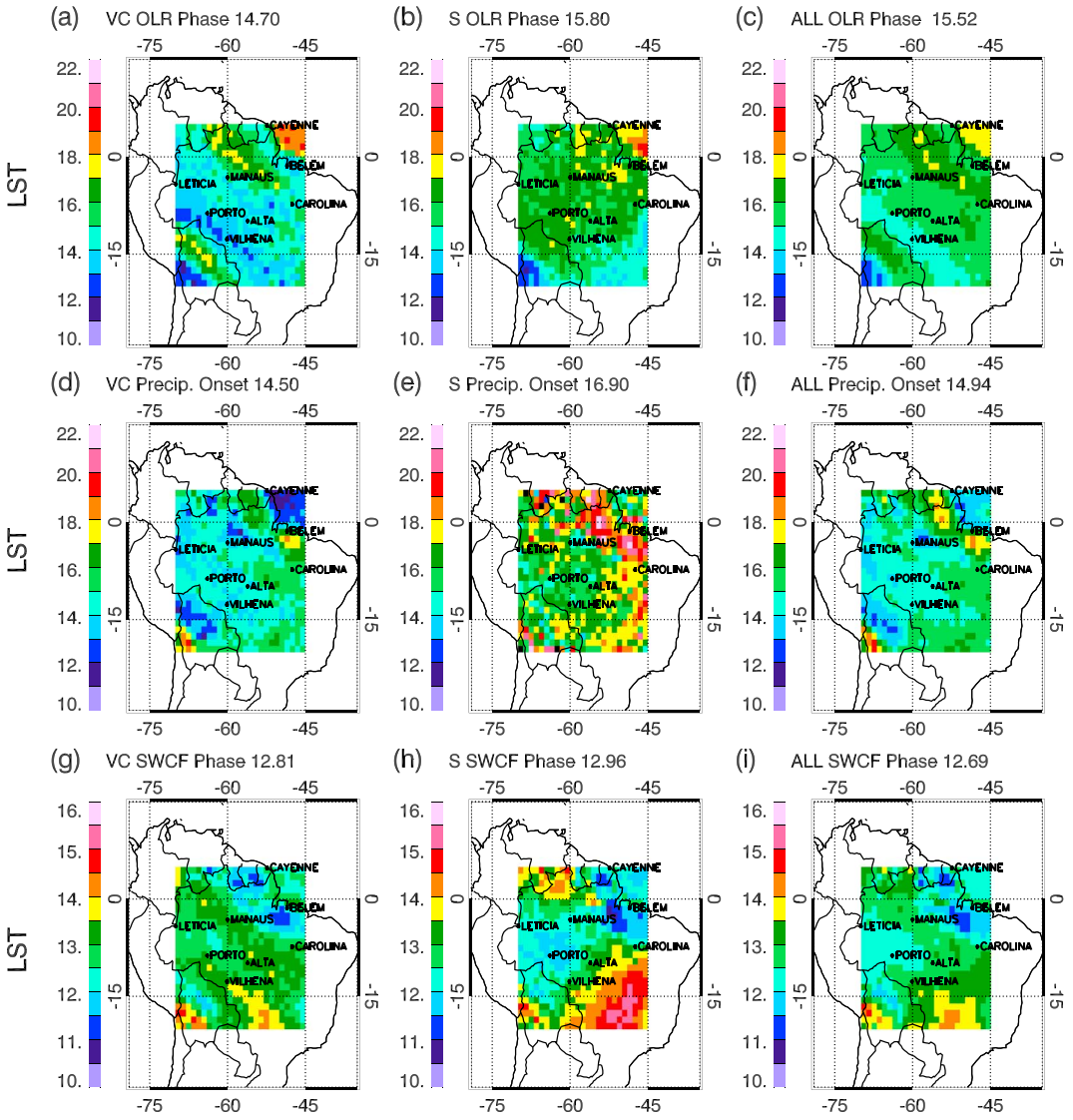

Figure 5. Composite spatial comparisons of diurnal timing statistics for the VC, S and ALL regimes in the wet season for (a–c) OLR phase, (d–f) precipitation onset, and (g–i) SWCF phase. The numerical value in each panel title provides the domain average of each diurnal cycle statistic. Contour intervals range from 1 h to one-half hour for SWCF.

RH is near 100% for all hours on VC days in the wet season, and S days exhibit larger diurnal amplitudes, maximizing above 90% before sunrise and minimizing near 60% between 12:00 and 15:00 LST for both seasons; however, on VC days in the dry season, RH only deviates from S days between 14:00 and 24:00 LST after convective initiation. The composite rainfall phase has three distinct modes in the wet season (08:00, 14:00, and 20:00 LST) compared to a single mode between 13:00 and 16:00 LST in the dry season (Figures 6c and 6d).

5.2. Relationship Between Atmospheric State and Convective Intensity

The relationships between convective parameters and convective intensity are briefly described below for 08:00 LST (morning) and 20:00 LST (evening) at six stations where reliable data are available for both times of day in the wet and dry seasons.

5.2.1. Thermodynamic Parameters

The results demonstrate statistically significant changes in the thermodynamic diagnostics by convective intensity in the wet (Figure 7) and dry (Figure 8) seasons. Overall, thermodynamic sensitivities to convective intensity are larger in the dry season than the wet season. Additionally, each station illustrates consistent results, albeit of varying magnitudes, despite the significant spatial variations in diurnal features.

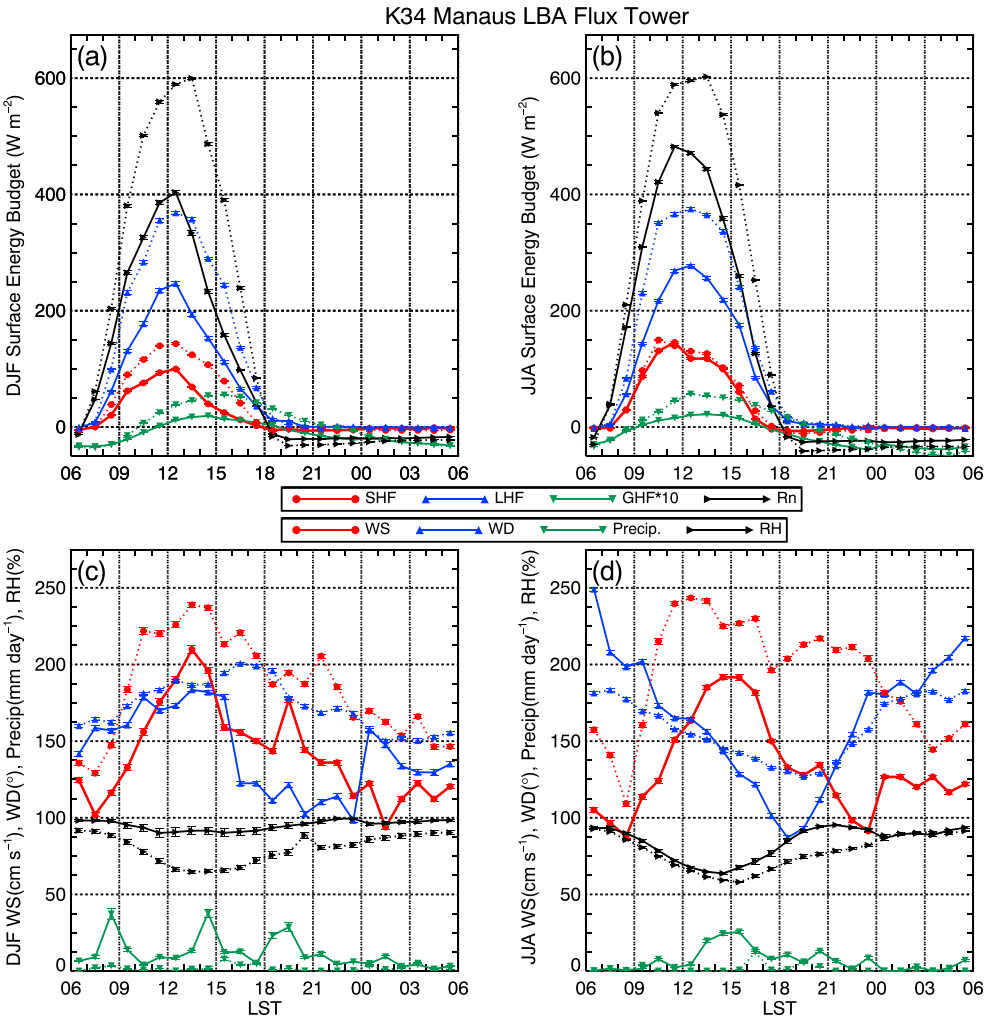

Figure 6. Diurnal cycle composites of surface energy budget terms: sensible heat flux (SHF), latent heat flux (LHF), and ground heat flux (GHF) multiplied by 10 and net radiation (Rn) and surface state variables: wind speed (WS), wind direction (WD), precipitation rate (Precip.), and relative humidity (RH) measured at 50 m above the ground during the LBA field campaign at a flux tower near Manaus, Brazil, split into VC days (solid line) and S days (dotted lines) for the (a, c) wet and (b, d) dry season.

The VC, MC, and LC regimes are associated with higher (lower) 08:00 LST values of UTH, LTH, LTS, and CAPE (LCL and TDEF) compared to N and S regimes in the wet and dry seasons for virtually all stations (Figures 7 and 8). Similarly, convective regimes are associated with higher (lower) 20:00 LST values of UTH, LTH, and LCL (CAPE and LTS) compared to N and S regimes for most stations. Stations near the coast (e.g., Manaus, Cayenne, and Belem) have the highest composite values of LTS and CAPE and the lowest composite values of TDEF and LCL at 08:00 LST across all regimes and seasons, indicating that these stations are more primed for afternoon convection.

Differences among parameters between 08:00 LST and 20:00 LST highlight the diurnal effects of convective intensity on atmospheric state. For VC regimes in the wet season, LTS decreases throughout the day and LTH decreases (increases) for Manaus, Porto Velho, and Vilhena (Cayenne, Belem, and Alta Floresta); and UTH, TDEF, and CAPE increase for most stations (Figures 7a–7f). For wet season S days, LCL, LTS, and CAPE increase and LTH and TDEF decrease. For dry season VC days and TDEF decrease and CAPE and UTH increase. For dry season S days, LTH, and TDEF decrease and CAPE, LCL, and LTS increase, whereas UTH decreases for interior stations and increases for coastal stations (Figures 8a–8f).

The physical mechanisms forcing differences in the diurnal cycles of OLR, LWCF, SWCF, and precipitation between the VC and S regimes can be inferred using the thermodynamic relationships in Figures 7 and 8

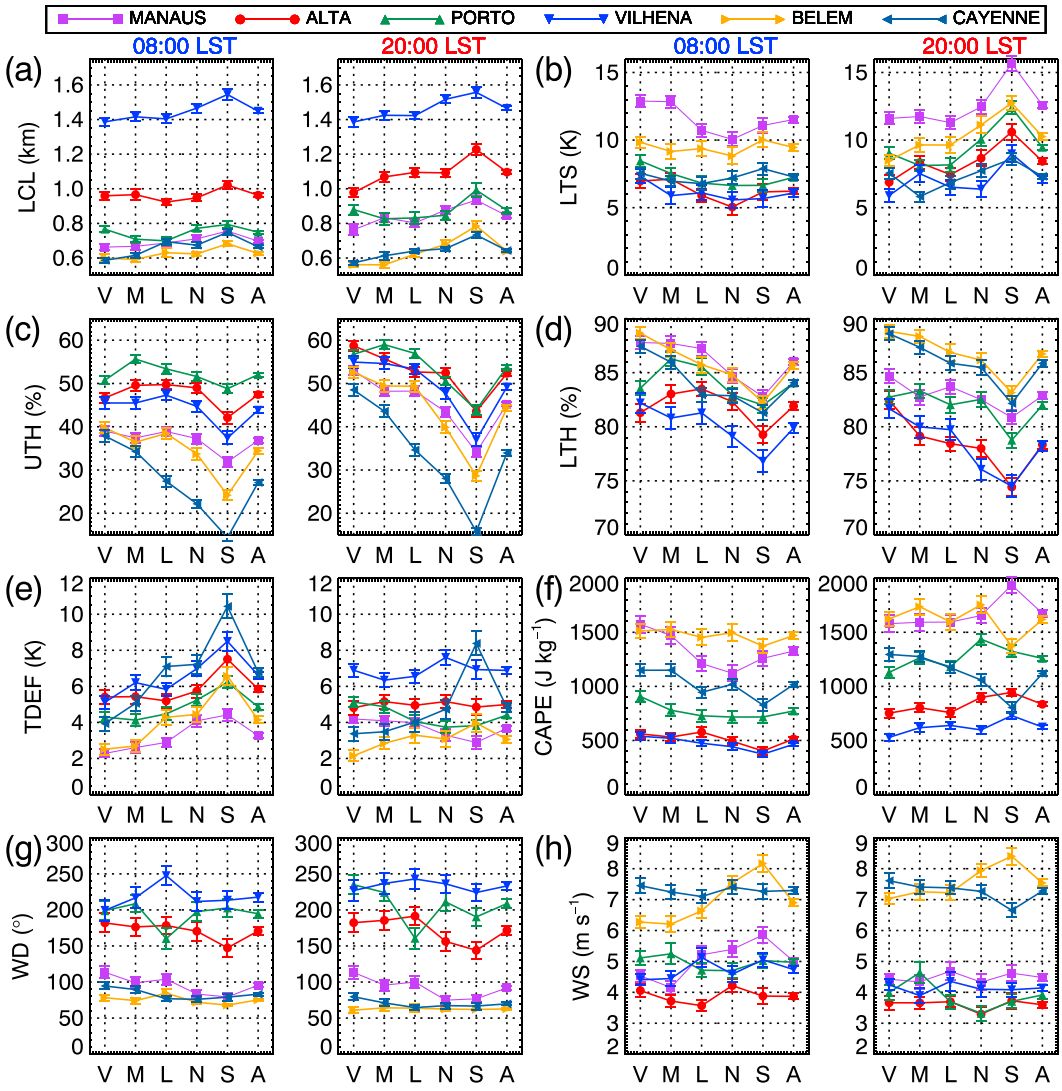

Figure 7. Composites of (a) LCL, (b) LTS, (c) UTH, (d) LTH, (e) TDEF, (f) CAPE, (g) WD, and (h) WS are shown for each convective intensity regime at 08:00 LST and 20:00 LST for the wet season: very convective (V), moderately convective (M), lowly convective (L), neutral (N), and stable (S).

combined with existing knowledge of convective processes. TDEF is largest at 08:00 LST in the S regime, indicating that more solar heating is required to overcome the larger negative buoyancy associated with a drier and more stable boundary layer. Further, shallow cumuli require more time to develop and moisten the region above the PBL on days with a lower LTH, which is related to an increase of TDEF and LCL. A later onset of precipitation in the S regime compared to the VC regime is consistent with these features suggesting a delayed convective initiation. *Sherwood* [1999]; *Soden* [2000], and *Zelinka and Hartmann* [2009] also documented the presence of anomalously high LTH several hours before convective initiation. In the dry season, convective initiation occurs several hours later than the wet season due in part to a larger morning TDEF from lower climatological humidity and also from a seasonal reduction in solar insolation.

5.2.2. Dynamic Parameters

Wind variables display weaker variations across the convective intensity regimes compared to thermodynamic variables; however statistically significant differences are found. Wind shear is an important mechanism that contributes to turbulent circulations and vertical velocity associated with convection [*Weisman and Klemp*, 1982; *Tompkins*, 2001]. The influence of the LLJ on convection in the Amazon depends on local effects and topography [*Machado et al.*, 2002]. It is difficult to define robust wind parameters across all stations and seasons for several reasons. Subseasonal variability in wind speed and direction is low due to small horizontal temperature

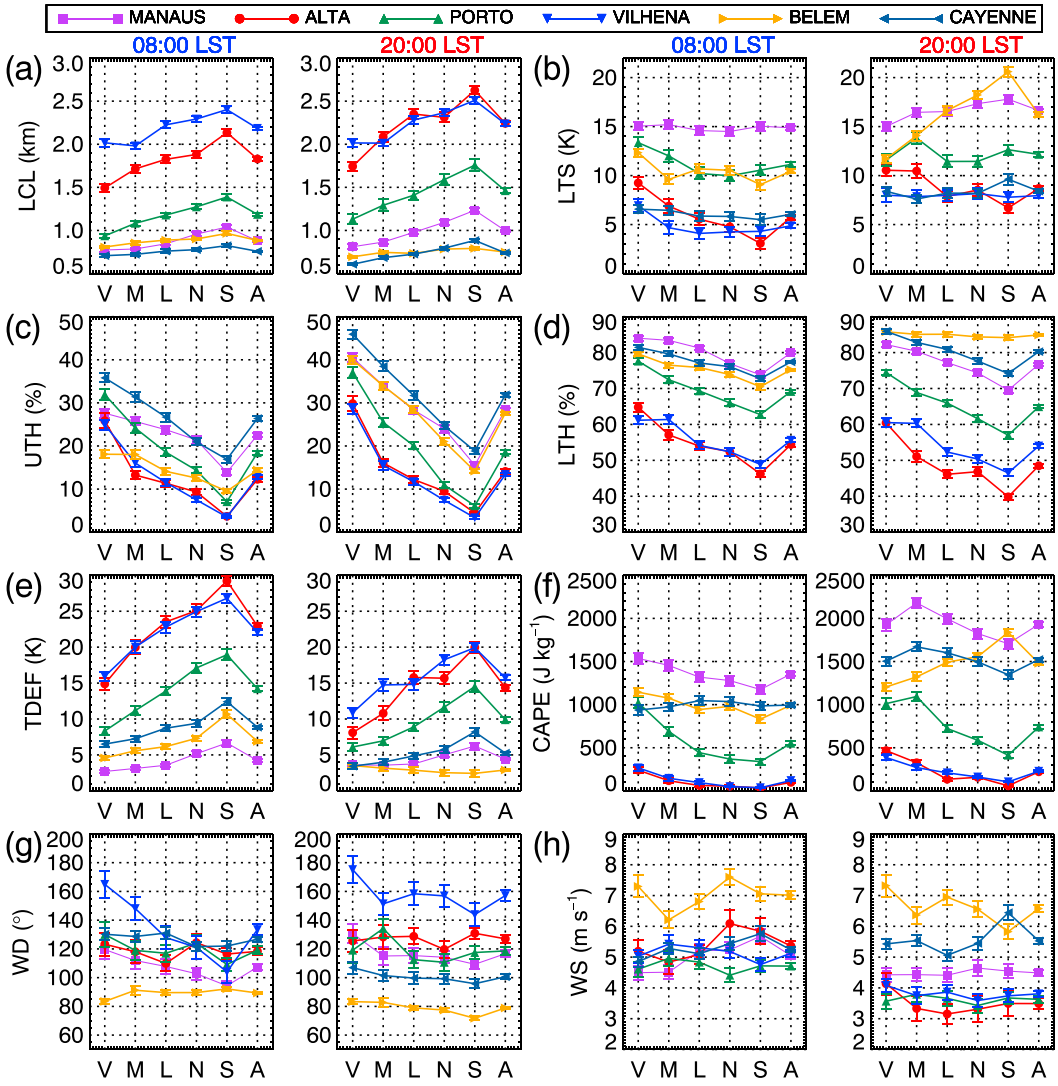

Figure 8. As in Figure 7 but for the dry season.

gradients in the Tropics. Also, seasonality and local effects influence wind profile characteristics (i.e., coastal stations compared to inland stations).

Lower tropospheric wind characteristics—direction and speed—between 1000 and 850 hPa are used to assess the change of low-level winds with convective intensity. Figure 7h reveals larger values of WS at 08:00 LST on S days for Belem and Manaus compared to VC days. In the dry season, WS is lower on VC days for Manaus and Alta Floresta at 08:00 LST; however, by 20:00 LST, values of WS are higher (lower) on VC days for Belem, Alta Floresta, and (Cayenne) (Figure 8h).

The 08:00 LST WD in the wet season on VC days is statistically significantly different from S days for Manaus, Cayenne, and Alta Floresta (Figure 7g). The 20:00 LST WD on VC days in Cayenne, Manaus, Porto, and Alta is different from S days by over one standard error (Figure 7g). In the dry season, the 08:00 LST WD on VC days in Vilhena and Manaus is more southerly than S days, whereas VC days in Belem are related to a slightly more northerly WD than the less convective regimes. The 20:00 LST WD on VC days in the dry season in Cayenne, Belem, Manaus, and Vilhena is different from S days by over one standard error (Figure 8g).

5.3. Relationship Between Convective Parameters and Diurnal Cycle Characteristics

The focus in this section is limited to describing the correlation between convective diurnal cycle statistics and 08:00 LST atmospheric state measured by radiosonde. *Sherwood* [1999] noted the large degree of covariability

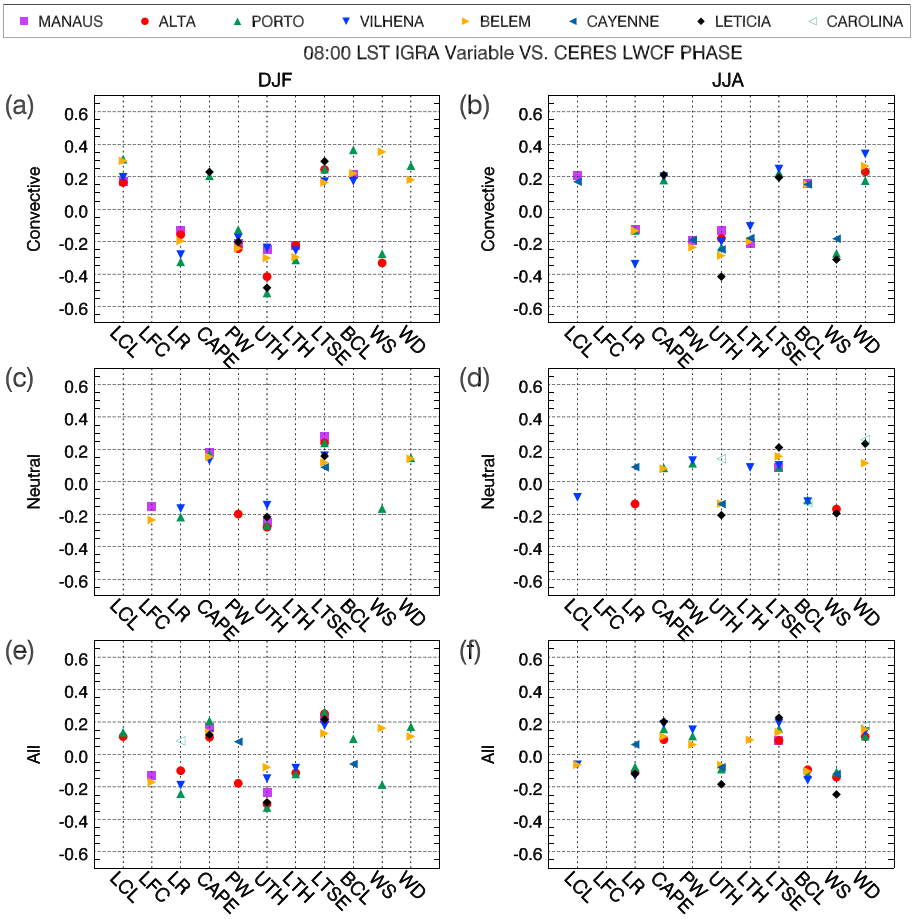

Figure 9. Pearson correlation coefficients between 08:00 LST convective parameters and LWCF phase for (a) wet season convective days, (b) dry season convective days, (c) wet season neutral days, (d) dry season neutral days, (e) wet season all days, and (f) dry season all days. Convective days include the VC, MC, and LC regimes; neutral days include the S and N regimes. Correlation coefficients significant at 90% are shown for all stations.

between important convective precursors, thus making it difficult to attribute the influence of individual precursors on the resulting convection. In the present study, a large number of variables are selected to compare their relative importance by season and station. No statistical attempt has been made to resolve the multicollinearity.

5.3.1. TOA Fluxes

Figure 9 displays the 90% statistically significant correlation coefficients between LWCF phase and convective parameters at 08:00 LST. While statistically significant relationships are found with other stability-relative parameters, LTS exhibits a significant relationship at most stations. The correlation results indicate that preconvective column moisture variables are the most robust predictors of afternoon LWCF phase. For convective regimes in both seasons, higher UTH at 08:00 LST is associated with an earlier LWCF phase with correlations ranging from 0.2 to 0.45 for most stations (Figures 9a and 9b). A higher LCL and lower LTH are also associated with a later LWCF phase for Belem, Vilhena, Alta Floresta, and Porto Velho. WD is significantly correlated to the LWCF phase for Belem and Porto Velho in the wet season and for Vilhena, Belem, Porto Velho, Alta Floresta, and Carolina in the dry season. Overall, correlations are weaker on neutral days for both seasons and weaker for the dry season than the wet season.

The correlation results (Figure 9) reveal an opposite relationship between LWCF phase and 08:00 LST humidity compared to the composite results (Figures 5, 7, and 8). The composite results indicate that 08:00 LST UTH is higher, and LWCF phase is later in the wet season on VC days compared to MC, LC, N, and S days. The correlation results indicate that mornings with higher UTH also have an earlier LWCF phase. These differing results highlight the importance of considering both the instantaneous and averaged relationships. The result suggests that above a certain humidity threshold, a separate process (related to how primed the PBL

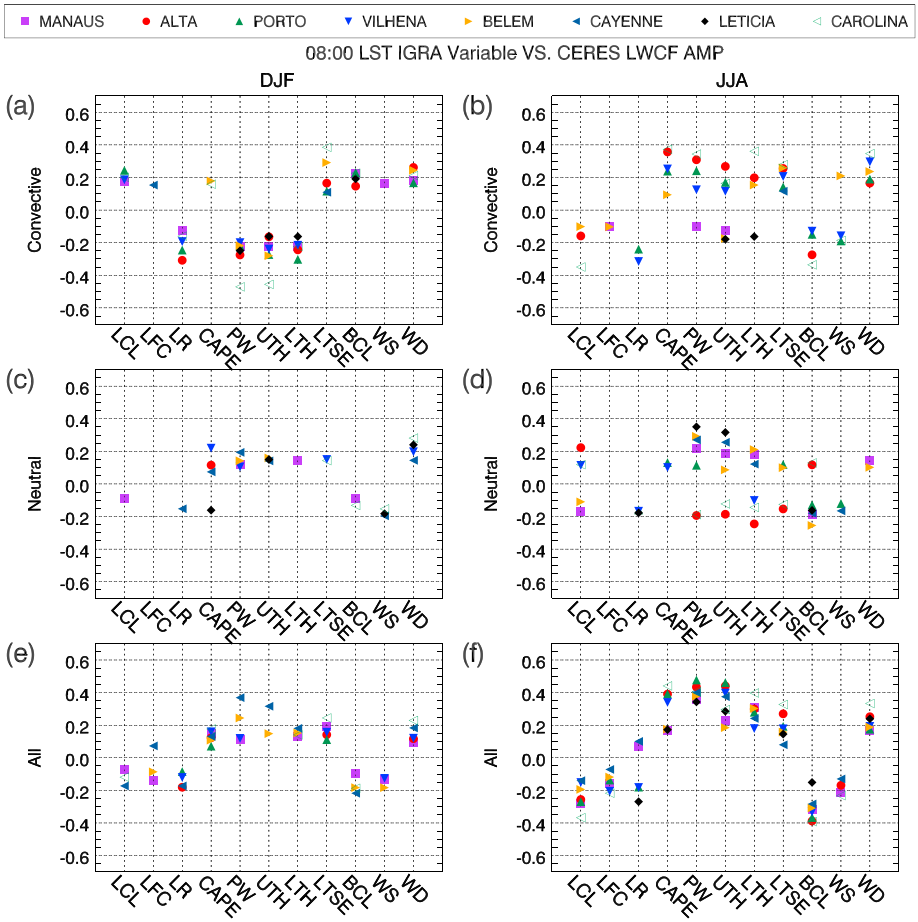

Figure 10. As in Figure 9 but for LWCF amplitude.

is for convective initiation) may be important but is removed when compositing. It is also possible that certain differences may result from nonlinearity between UTH and clear-sky OLR flux or a bias in CERES clear-sky sampling [*Loeb et al.*, 2009]. In the neutral regime, a higher LTS and lower UTH are related to a later LWCF phase for most stations; however, correlations are weaker (Figures 9c and 9d). Considering all regimes together, the correlation of LWCF phase with atmospheric state is consistent between stations and seasons but with lower values than convective days.

The correlation coefficients between LWCF amplitude and morning atmospheric state are shown in Figure 10. In the wet season, lower values of morning humidity are associated with larger LWCF amplitudes on convective days, with correlations ranging between −0.15 and −0.45 (Figure 10a). Higher morning humidity is associated with larger morning cloud fractions reducing the potential for diurnal changes in cloud fraction and LWCF. Lower morning humidity is accompanied by less cloudiness and a lower LWCF and a larger potential to increase through the day (not shown). The sign of this relationship is flipped considering convective days in the dry season and neutral days for both seasons (Figures 10b–10d), and the LWCF amplitude is positively correlated with column humidity except for Manaus and Leticia where humidity is significantly higher than southern stations (Figure 8d) and for the driest stations in the dry season neutral regime where convection is rare and LWCF amplitudes are primarily related to low-level cumulus cloud formation (Figure 10d). On convective days in the dry season and neutral days in both seasons, morning cloudiness and LWCF are not large enough to significantly reduce the potential for a large amplitude diurnal cycle in the presence of higher column moisture. We speculate that a portion of increased morning cloud fraction during the wet season is from lingering anvil clouds from the previous day's convection that dissipates more slowly due to the higher UTH. Alternatively, the presence of morning clouds may be a function of the large-scale atmospheric state and may be advected, produced, or at least favored when conditions are favorable for stronger diurnal cycles.

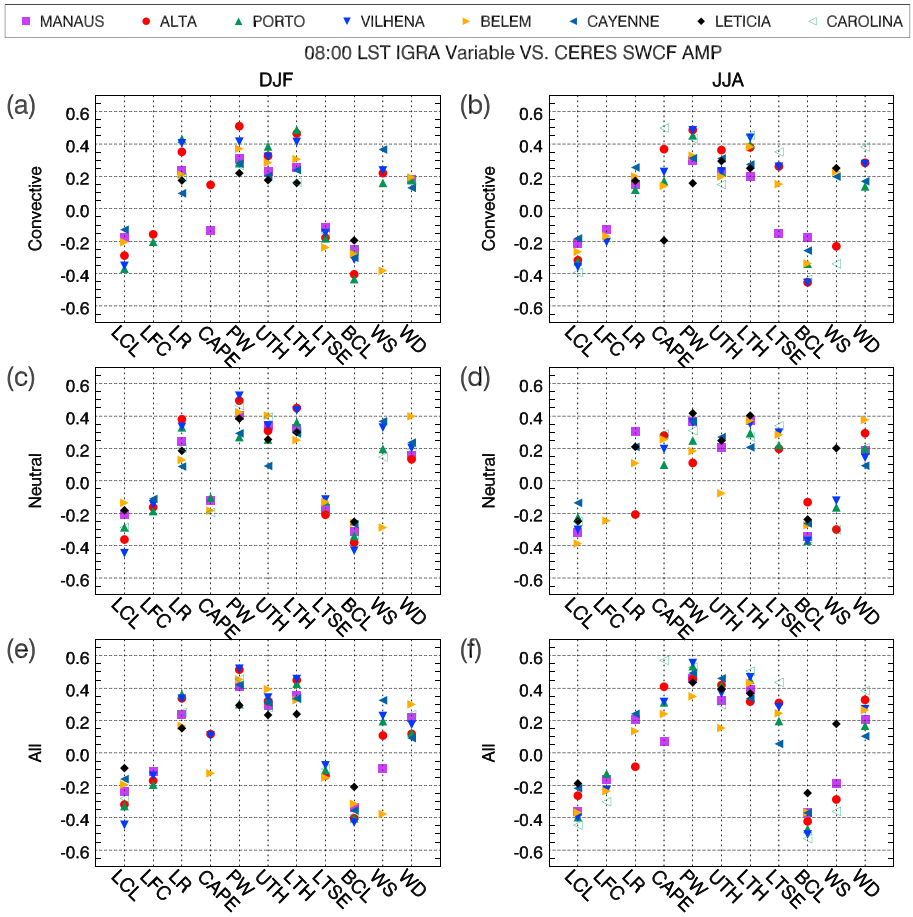

Figure 11. As in Figure 9 but for SWCF amplitude.

Considering all regimes, higher morning values of UTH, LTH, PW, and CAPE are significantly related to larger LWCF diurnal amplitudes for both seasons (Figures 10e and 10f). The larger number of significant correlations is related to the large number of samples when convective and neutral days are combined. The sign of the correlations is consistent with wet season neutral days but is inconsistent with wet season convective days. Figure 10 highlights significant differences in the seasonality of the relationship between the convective diurnal cycle and atmospheric state. To accurately simulate the nature of convection and the convective diurnal cycle in the Amazon, models must simulate these seasonal differences in convective behavior.

The correlation coefficients between SWCF amplitude and atmospheric state are shown in Figure 11. Correlations are stronger and more robust than longwave diurnal cycle statistics, which is due partially because shortwave fluxes are not influenced by the nighttime portion of the diurnal cycle dominated by propagating features and mesoscale processes. For convective regimes in both seasons, correlations between SWCF amplitude and PW, UTH, and LTH (LCL and BCL) range from 0.15 to 0.5 to (-0.15 to -0.5) (Figures 11a and 11b). However, for LTS and CAPE, the sign and magnitude of the correlation with SWCF amplitude is seasonally dependent.

In the wet season, lower values of LTS are associated with a larger SWCF amplitude (Figure 11a). In the dry season, for stations where moisture availability is relatively scarce, LTS and CAPE are positively correlated with SWCF amplitude ranging from 0.2 to 0.4 (Figure 11b). WD and WS also become important factors for interior stations in the dry season and coastal stations in DJF, which is possibly related to mesoscale advection of moisture (Figures 11a and 11b).

5.3.2. Precipitation

Diurnal cycle characteristics of precipitation show stronger correlations with atmospheric state than the TOA fluxes. Figures 5 and 6 illustrate significant composite changes in the precipitation onset and duration with convective intensity, whereas precipitation phase shows little change. However, the instantaneous

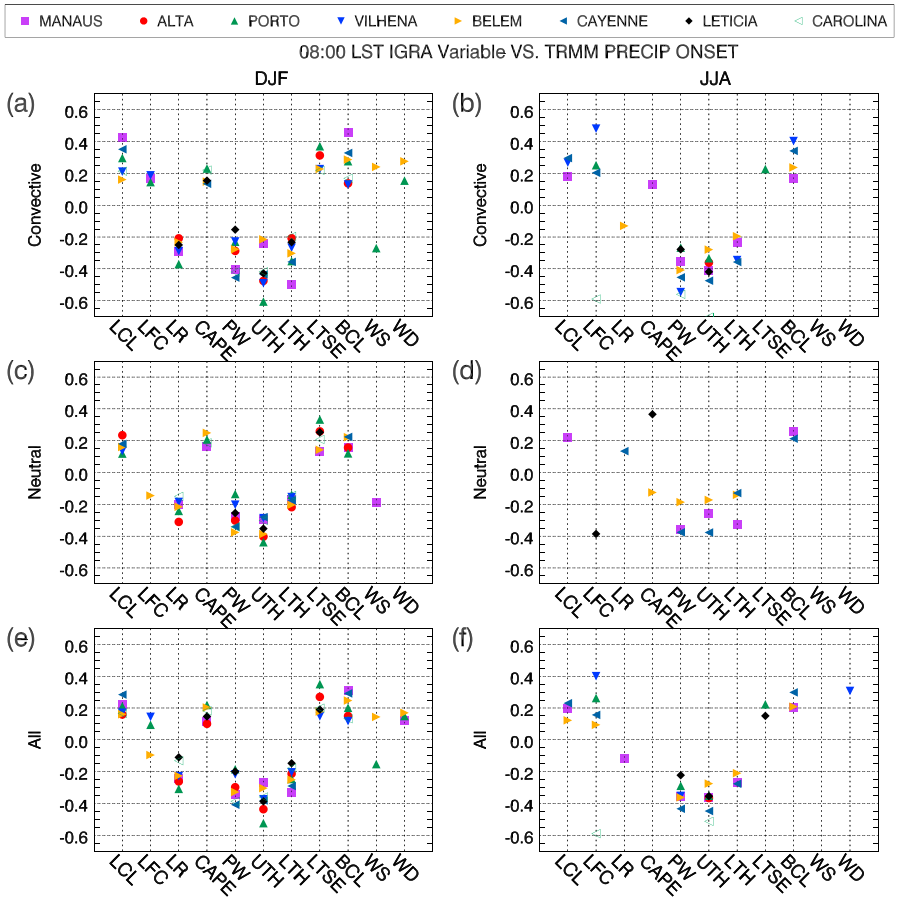

Figure 12. As in Figure 9 but for precipitation onset.

correlation analysis reveals similar results for precipitation phase (not shown), precipitation onset time (Figure 12), and precipitation duration (not shown).

Statistically significant correlations are found between many variables and the onset of precipitation for all stations (Figure 12). In convective regimes, precipitation onset in the wet season is strongly anticorrelated with 08:00 LST column moisture variables with correlations ranging from -0.2 to -0.6 for all stations; more moisture is associated with earlier precipitation onset. Higher values of LTS and BCL are associated with a later precipitation onset. CAPE and LTS are positively correlated with precipitation onset for Manaus, Belem, Porto Velho, Leticia, and Carolina. In neutral regimes and in the dry season, most variables show less robust correlations with precipitation onset than the wet season, which is related to less valid days where precipitation rate exceeds 10 mm d^{-1}.

6. Discussion

6.1. Implications

Tropospheric humidity at 08:00 LST is the best correlated atmospheric state variable to variations in the convective diurnal cycle in nearly all cases. The absolute value of 08:00 LST composite tropospheric humidity is 20–40% higher on VC days compared to S days, depending on station and season. This finding corroborates previous studies. *Sherwood* [1999] showed that moisture above the boundary layer is more robust than CAPE at explaining convective characteristics over warm tropical oceans [*Sherwood*, 1999]. Three-dimensional cloud-resolving simulations also indicate that LTH was an influential factor affecting tropical convection [*Tompkins*, 2001; *Derbyshire et al.*, 2004]. *Sobel et al.* [2004] further showed that increased LTH leads precipitation by 1–3 h.

The results have implications for understanding model biases related to CAPE-based convective closure and triggering criteria. *Suhas and Zhang* [2014] and *Wang et al.* [2015] showed that convective triggers using

undiluted parcels to calculate CAPE perform poorly relative to triggers that incorporate free tropospheric moisture and large-scale forcings. *Suhas and Zhang* [2014] suggest that a balanced treatment of free tropospheric humidity, large-scale destabilization, and surface forcings is necessary for producing accurate initiation. This work provides further observational basis for such claims and serves as motivation to include metrics such as LTH and UTH into convective closure and triggering parameterizations.

The relationships between convective precursors and the convective diurnal cycle are crucial for an improved understanding of the physical mechanisms and feedbacks that control convection in the Amazon [*Machado et al*., 2014]. Upper level atmospheric observations are scarce in the Amazon region, and scientific understanding of the physical mechanisms responsible for the initiation of Tropical moist convection is relatively poor [e.g., *Betts*, 2000]. Understanding of the convective controls during the Amazon wet season is especially poor because the atmosphere is so close to saturation it becomes unstable to moist processes on a range of scales [*Betts et al*., 2009] and commonly used convection schemes are not able to accurately capture the evolution of the Amazon convective diurnal cycle.

6.2. Caveats

Potential biases exist in the calculations of the convective parameters from radiosonde observations and in the selection of convective parameters to analyze. Parameters that do not depend on arbitrary vertical levels or resolutions are selected whenever possible to avoid additional sources of bias. Also, radiosonde observations occur twice daily at approximately 20:00 LST and 08:00 LST; these times are not ideal for capturing the environmental conditions when convective initiation is imminent. These times, however, are suitable to analyze atmospheric preconditioning and the atmospheric response to convection. The temporal restriction must be considered when interpreting the results.

Despite its importance to convective initiation, subgrid scale variability of satellite-observed fluxes and precipitation is not accounted for with the current methodology. Therefore, on days with localized convection, local features may obscure the relationships between instantaneous radiosonde measurements and diurnal cycle characteristics of TOA fluxes or precipitation. It is only possible to identify larger-scale physical relationships associated with the most significant convective events; however, if poorly simulated by models, these relationships have high potential impact on the climatological energy and water budget. Measurements from field campaigns or footprint-level satellite observables could be used to address subgrid effects.

The high degree of covariability among the thermodynamic and dynamic precursors presents a difficult problem. With the current methodology, it is not possible to separate the influence of individual variables on convective intensity from their influence on each other nor is it possible to identify nonlinear relationships among them. As noted by *Sherwood* [1999], one way to account for this effect is to select physically logical criteria to test hypotheses on the physical mechanisms controlling convection. This adds a subjective nature to the current framework, which can be minimized by advancing our understanding of moist convection through field campaigns or results from large eddy simulation, and therefore should be routinely evaluated as scientific knowledge progresses.

7. Summary and Conclusion

The relationship between convective intensity and diurnal cycle characteristics is investigated in the Amazon by collocating satellite, flux tower, and radiosonde observations over an 11 year period. The results indicate statistically significant relationships between convective intensity, diurnal cycle, and atmospheric state. Instantaneous correlation results reveal relationships not found in the composite results, highlighting the importance of considering each day as a diurnal cycle process as opposed to the conventional averaging approach.

Several robust composite relationships are found between convective intensity and the diurnal cycle. Convection decreases the diurnal amplitude of surface fluxes, particularly LHF, due to the earlier onset of clouds and precipitation and higher background humidity, which reduces solar insolation at the surface. This effect is larger in the wet season due to more frequent and intense convection that occurs earlier in the day on average. Near-surface wind speeds are 10–20% higher on S days than VC days for both seasons and all times of day. Morning WD is more sensitive to convective intensity in the dry season, and afternoon WD is more sensitive to convective intensity in the wet season. Maximum composite rainfall occurs at three

preferential modes in the wet season (08:00, 14:00, and 20:00 LST) compared to a single, broader mode between 13:00 and 16:00 LST in the dry season.

The domain-averaged composite OLR phase occurs 1–2 h earlier on very convective days compared to stable days in the wet season. Clouds grow more rapidly on convective days due to lower values of TDEF, LCL and LFC, which are related to higher humidity. Composite LWCF phase occurs 2 h later on very convective days in both seasons compared to stable days. Rainfall persists about two times longer on VC days compared to S days during the wet and dry seasons. Precipitation onset also occurs 2 to 4 h earlier on very convective days; however, precipitation phase is less sensitive to convective intensity. The composite diurnal amplitude increases with convective intensity for all variables and seasons, but the dry season diurnal amplitude varies more between the regimes.

Spatial composites reveal complex features of the diurnal cycle across the Amazon. The propagation of the coastal squall line inland is visible in the OLR phase composite for VC days but not for S days. The earliest OLR phase on VC days occurs along the northeast coast of Brazil and in the Rondônia region in southwestern Brazil, occurring just after noon. Spatial composites of SWCF phase show a detailed view of the progression of composite daytime cloud features, with the earliest values occurring before noon inland from the northeast coast and large spatial differences between the regimes in other areas.

The results show that the most robust relationships are between the diurnal cycle of convection and column moisture. Specifically, instantaneous correlation results show higher values of morning tropospheric humidity that are related to an earlier precipitation phase, earlier LWCF phase, later OLR phase, longer precipitation duration, and increased SWCF amplitude for all seasons and most stations. LWCF amplitude displays a seasonally and regionally dependent relation to humidity. On convective days in the dry season and neutral regimes, higher 08:00 LST humidity is related to larger diurnal amplitudes of LWCF, and on convective days in the wet season the relationship is opposite because morning cloudiness and humidity restrict the potential for a large LWCF amplitude.

Larger morning CAPE is related to increased precipitation and LWCF amplitudes, larger SWCF amplitudes in the dry season, a later precipitation onset in the wet season, and a later LWCF phase. Thus, morning CAPE alone cannot fully discriminate between strong and weak convection nor can it discriminate between convective and nonconvective days in the Amazon. The results indicate that convective parameterizations solely based on CAPE are not well suited for the Amazon region, especially in the wet season.

Despite the large spatial variations in the Amazonian convective diurnal cycle characteristics and the varying mechanisms of convective triggering, the relationships between the convective diurnal cycle and atmospheric state are remarkably consistent across all eight stations. This indicates that the relationships between the convective diurnal cycle and preconvective column moisture are robust despite the multitude of influencing factors as follows: large-scale flow, land-ocean interactions, initial conditions, local topography, and surface-type differences [*Silva Dias et al*., 2002].

The sensitivity of rainfall and radiative flux diurnal statistics to morning precursors, including its seasonality, must be captured by convective parameterizations [*Sherwood*, 1999]. An approach similar to the methodology presented here is underway to evaluate and explain diurnal cycle characteristics in models. Identifying the observed relationships between the convective diurnal cycle and convective precursors is a critical step toward improving model simulations of convection.

Acknowledgments

This work was supported by the NASA Energy and Water Cycle Studies program through grant NNH10ZDA001N. CERES data used in this study are stored at the Atmospheric Science Data Center (ASDC) at NASA Langley Research Center. TRMM 3B42 precipitation data were downloaded online (http://mirador.gsfc.nasa.gov). IGRA radiosonde data were downloaded online (http://www.ncdc.noaa.gov/data-access/weather-balloon/integrated-global-radiosonde-archive). LBA flux tower data from the Manaus K34 site were downloaded online (https://daac.ornl.gov/cgi-bin/dsviewer.pl?ds_id=1174).

References

Allan, R. P., K. P. Shine, A. Slingo, and J. A. Pamment (1999), The dependence of clear-sky outgoing longwave radiation on surface temperature and relative humidity, *Q. J. R. Meteorol. Soc.*, *125*(B), 2103–2126.

Arakawa, A. (2004), The cumulus parameterization problem: Past, present, and future, *J. Clim.*, *217*, 2493–2525.

Berens, P. (2009), CircStat: A Matlab toolbox for circular statistics, *J. Stat. Softw.*, *31*, 10.

Bergman, J. W., and M. L. Salby (1997), The role of cloud diurnal variations in the time-mean energy budget, *J. Clim.*, *10*, 1114–1124.

Betts, A. K. (2000), Idealized model for equilibrium boundary layer over land, *J. Hydrometeorol.*, *1*(6), 507–523.

Betts, A. K., and C. Jakob (2002a), Evaluation of the diurnal cycle of precipitation, surface thermodynamics, and surface fluxes in the ECMWF model using LBA data, *J. Geophys. Res.*, *107*(D20), 8045, doi:10.1029/2001JD000427.

Betts, A. K., and C. Jakob (2002b), Study of diurnal cycle of convective precipitation over Amazonia using a single column model, *J. Geophys. Res.*, *107*(D23), 4732, doi:10.1029/2002JD002264.

Betts, A. K., J. Fuentes, M. Garstang, and J. H. Ball (2002), Surface diurnal cycle and boundary layer structure over Rondônia during the rainy season, *J. Geophys. Res.*, *107*(D20), 8065, doi:10.1029/2001JD000356.

Betts, A. K., G. Fisch, C. von Randow, M. A. F. Silva Dias, J. C. P. Cohen, R. da Silva, and D. R. Fitzjarrald (2009), The Amazonian boundary layer and mesoscale circulations, in *Amazonia and Global Change*, *Geophys. Monogr. Ser.*, vol. 186, edited by M. Keller et al., pp. 163–181, AGU, Washington, D. C.

Bolton, D. (1980), The computation of equivalent potential temperature, *Mon. Weather Rev.*, *108*, 1046–1053.

Chaboureau, J.-P., F. Guichard, J.-L. Redelsperger, and J.-P. Lafore (2004), The role of stability and moisture in the diurnal cycle of convection over land, *Q. J. R. Meteorol. Soc.*, *130*, 3105–3117.

Cohen, J. C. P., M. A. F. Silva Dias, and C. A. Nobre (1995), Environmental conditions associated with Amazonian squall lines: A case study, *Mon. Weather Rev.*, *123*, 3163–3174.

Collier, J. C., and K. P. Bowman (2004), Diurnal cycle of tropical precipitation in a general circulation model, *J. Geophys. Res.*, *109*, D17105, doi:10.1029/2004JD004818.

Dai, A. G. (2001), Global precipitation and thunderstorm frequencies. Part II: Diurnal variations, *J. Clim.*, *14*, 1112–1128.

Dai, A., and K. E. Trenberth (2004), The diurnal cycle and its depiction in the community climate system model, *J. Clim.*, *17*, 930–951.

De Gonçalves, L. G. G., et al. (2013), Overview of the large-scale biosphere-atmosphere experiment in Amazonia data model intercomparison project (LBA-DMIP), *Agric. Forest Meteorol.*, *182*(183), 111–127.

Derbyshire, S. H., I. Beau, P. Bechtold, J.-Y. Grandpeix, J.-M. Piriou, J.-L. Redelsperger, and P. M. Soares (2004), Sensitivity of moist convection to environmental humidity, *Q. J. R. Meteorol. Soc.*, *130*, 3055–3080.

Dirmeyer, P. A. (2011), The terrestrial segment of soil moisture–climate coupling, *Geophys. Res. Lett.*, *38*, L16702, doi:10.1029/2011GL048268.

Dodson, J. B., and P. C. Taylor (2016), Sensitivity of Amazonian TOA flux diurnal cycle composite monthly variability to choice of reanalysis, *J. Geophys. Res. Atmos.*, *121*, 4404–4428, doi:10.1002/2015JD024567.

Doelling, D. R., N. G. Loeb, D. F. Keyes, M. L. Nordeen, D. Morstad, C. Nguyen, B. A. Wielicki, D. F. Young, and M. Sun (2013), Geostationary enhanced temporal interpolation for CERES flux products, *J. Atmos. Oceanic Technol.*, *30*, 1072–1090.

Durre, I., R. S. Vose, and D. B. Wuertz (2006), Overview of the Integrated Global Radiosonde Archive, *J. Clim.*, *19*, 53–68.

Durre, I., R. S. Vose, and D. B. Wuertz (2008), Robust automated quality assurance of radiosonde temperatures, *J. Appl. Meteorol. Climatol.*, *47*, 2081–2095.

Ek, M. B., and A. A. M. Holtslag (2004), Influence of soil moisture on boundary layer cloud development, *J. Hydrometeorol.*, *5*, 86–99.

Folkins, I., T. Mitovski, and J. R. Pierce (2014), A simple way to improve the diurnal cycle in convective rainfall over land in climate models, *J. Geophys. Res. Atmos.*, *119*, 2113–2130, doi:10.1002/2013JD020149.

Gray, W. M., and R. W. Jacobson Jr. (1977), Diurnal variation of deep cumulus convection, *Mon. Weather Rev.*, *105*, 1171–1188.

Holtslag, A. A., and C.-H. Moeng (1991), Eddy diffusivity and countergradient transport in the convective atmospheric boundary layer, *J. Atmos. Sci.*, *48*, 1690–1698.

Itterly, K. F., and P. C. Taylor (2014), Evaluation of the tropical TOA flux diurnal cycle in MERRA and ERA-Interim retrospective analyses, *J. Clim.*, *27*(13), 4781–4796.

Janowiak, J. E., P. A. Arkin, and M. Morrissey (1994), An examination of the diurnal cycle in oceanic tropical rainfall using satellite and in situ data, *Mon. Weather Rev.*, *122*, 2296–2311.

Kuang, Z. M., and C. S. Bretherton (2006), A mass flux scheme view of a high-resolution simulation of a transition from shallow to deep cumulus convection, *J. Atmos. Sci.*, *63*(7), 1895–1909.

Kummerow, C., W. Barnes, T. Kozu, J. Shiue, and J. Simpson (1998), The Tropical Rainfall Measuring Mission (TRMM) sensor package, *J. Atmos. Oceanic Technol.*, *15*, 809–817.

Liebmann, B., J. A. Marengo, J. D. Glick, V. E. Kousky, I. C. Wainer, and O. Massambani (1998), A comparison of rainfall, outgoing longwave radiation, and divergence over the Amazon Basin, *J. Clim.*, *11*, 2898–2909.

Lin, X., D. A. Randall, and L. D. Fowler (2000), Diurnal variability of the hydrologic cycle and radiative fluxes: Comparisons between observations and a GCM, *J. Clim.*, *13*, 4159–4179.

Loeb, N. G., B. A. Wielicki, D. R. Doelling, G. L. Smith, D. F. Keyes, S. Kato, N. Manalo-Smith, and T. Wong (2009), Toward optimal closure of the Earth's Top-of-Atmosphere radiation budget, *J. Clim.*, *22*, 748–766.

Machado, L. A. T., H. Laurent, and A. A. Lima (2002), Diurnal march of the convection observed during TRMM-WETAMC/LBA, *J. Geophys. Res.*, *107*(D20), 8064, doi:10.1029/2001JD000338.

Machado, L. A. T., et al. (2014), The Chuva project: How does convection vary across Brazil?, *Bull. Am. Meteorol. Soc.*, *95*, 1365–1380.

Nesbitt, S. W., and E. J. Zipser (2003), The diurnal cycle of rainfall and convective intensity according to three years of TRMM measurements, *J. Clim.*, *16*, 1456–1475.

Pereira, L. G., and S. A. Rutledge (2006), Diurnal cycle of shallow and deep convection for a tropical land and an ocean environment and its relationship to synoptic wind regimes, *Mon. Weather Rev.*, *134*, 2688–2701.

Randall, D., M. Khairoutdinov, A. Arakawa, and W. Grabowski (2003), Breaking the cloud parameterization deadlock, *Bull. Am. Meteorol. Soc.*, *84*(11), 1547–1562.

Rickenbach, T. M. (2004), Nocturnal cloud systems and the diurnal variation of clouds and rainfall in southwestern Amazonia, *Mon. Weather Rev.*, *132*, 1201–1219.

Saleska, S. R., H. R. da Rocha, A. R. Huete, A. D. Nobre, P. Artaxo, and Y. E. Shimabukuro (2013), LBA-ECO CD-32 flux tower network data compilation, Brazilian Amazon: 1999–2006, data set. [Available at http://daac.ornl.gov, from Oak Ridge National Laboratory Distributed Active Archive Center, Oak Ridge, Tennessee, USA.]

Santanello, J. A., Jr., C. Peters-Lidard, S. V. Kumar, C. Alonge, and W.-K. Tao (2009), A modeling and observational framework for diagnosing local land-atmosphere coupling on diurnal time scales, *J. Hydrometeorol.*, *10*(3), 577–599.

Schlemmer, L., C. Hohenegger, J. Schmidli, C. S. Bretherton, and C. Schär (2011), An idealized cloud-resolving framework for the study of midlatitude diurnal convection over land, *J. Atmos. Sci.*, *68*, 1041–1057.

Sherwood, S. C. (1999), Convective precursors and predictability in the tropical western Pacific, *Mon. Weather Rev.*, *127*, 2977–2991.

Silva Dias, M. A. F., et al. (2002), Cloud and rain processes in a biosphere–atmosphere interaction context in the Amazon region, *J. Geophys. Res.*, *107*(D20), 8072, doi:10.1029/2001JD000335.

Smith, T. M., P. A. Arkin, J. J. Bates, and G. J. Huffman (2006), Estimating bias of satellite-based precipitation estimates, *J. Hydrometeorol.*, *7*(5), 841–856.

Sobel, A. H., S. E. Yuter, C. S. Bretherton, and N. G. Kiladis (2004), Large-scale meteorology and deep convection during TRMM KWAJEX, *Mon. Weather Rev.*, *132*(2), 422–444.

Soden, B. J. (2000), The diurnal cycle of convection, clouds and water vapor in the tropical upper troposphere, *Geophys. Res. Lett.*, *27*(15), 2173–2176, doi:10.1029/2000GL011436.

Strong, C., J. D. Fuentes, M. Garstang, and A. K. Betts (2005), Daytime cycle of low-level clouds and the tropical convective boundary layer in southwestern Amazonia, *J. Appl. Meteorol.*, *44*, 1607–1619.

Suhas, E., and G. J. Zhang (2014), Evaluation of trigger functions for convective parameterization schemes using observations, *J. Clim.*, *27*(20), 7647–7666.
Tanaka, L. M. d. S., P. Satyamurty, and L. A. T. Machado (2014), Diurnal variation of precipitation in central Amazon Basin, *Int. J. Climatol.*, *34*, 3574–3584.
Tawfik, A. B., and P. A. Dirmeyer (2014), A process-based framework for quantifying the atmospheric preconditioning of surface-triggered convection, *Geophys. Res. Lett.*, *41*, 173–178, doi:10.1002/2013GL057984.
Tawfik, A. B., P. A. Dirmeyer, and J. A. Santanello Jr. (2015), The heated condensation framework. Part I: Description and Southern Great Plains case study, *J. Hydrometeorol.*, *16*, 1929–1945.
Taylor, P. C. (2012a), Tropical outgoing longwave radiation and longwave cloud forcing diurnal cycles from CERES, *J. Atmos. Sci.*, *69*(12), 3652–3669.
Taylor, P. C. (2012b), The role of clouds: An introduction and rapporteur report, *Surv. Geophys.*, 1–9.
Taylor, P. C. (2014a), Variability of monthly diurnal cycle composites of TOA radiative fluxes in the Tropics, *J. Atmos. Sci.*, *71*(2), 754–766.
Taylor, P. C. (2014b), Variability of regional TOA flux diurnal cycle composites at the monthly time scale, *J. Atmos. Sci.*, *71*(9), 3484–3498.
Tompkins, A. M. (2001), Organization of Tropical convection in low vertical wind shears: The role of water vapor, *J. Atmos. Sci.*, *58*, 529–545.
Trier, S. B., F. Chen, K. W. Manning, M. A. LeMone, and C. A. Davis (2008), Sensitivity of the PBL and precipitation in 12-day simulations of warm-season convection using different land surface models and soil wetness conditions, *Mon. Weather Rev.*, *136*(7), 2321–2343.
Van Heerwaarden, C. C., J. V.- G. de Arellano, and A. J. Teuling (2010), Land-atmosphere coupling explains the link between pan evaporation and actual evapotranspiration trends in a changing climate, *Geophys. Res. Lett.*, *37*, L21401, doi:10.1029/2010GL045374.
Wang, Y.-C., H.-L. Pan, and H.-H. Hsu (2015), Impacts of the triggering function of cumulus parameterization on warm-season diurnal rainfall cycles at the Atmospheric Radiation Measurement Southern Great Plains site, *J. Geophys. Res. Atmos.*, *120*, 681–702, doi:10.1002/2015JD023337.
Weisman, M. L., and J. B. Klemp (1982), The dependence of numerically simulated convective storms on vertical wind shear and buoyancy, *Mon. Weather Rev.*, *110*, 504–520.
Yang, G.-Y., and J. Slingo (2001), The diurnal cycle in the tropics, *Mon. Weather Rev.*, *129*, 784–801.
Zelinka, M. D., and D. L. Hartmann (2009), Response of humidity and clouds to tropical deep convection, *J. Clim.*, *22*, 2389–2404.
Zhang, Y., and S. A. Klein (2010), Mechanisms affecting the transition from shallow to deep convection over land: Inferences from observations of the diurnal cycle collected at the ARM Southern Great Plains site, *J. Atmos. Sci.*, *67*, 2943–2959.